

DESIGN AND DEVELOPMENT OF A MICROFLUIDIC DEVICE TO MONITOR  
IRON BINDING DYNAMICS IN IRON TRANSPORT PROTEINS

by

GÖKŞİN LİU

Submitted to the Graduate School of Engineering and Natural Sciences

in partial fulfillment of

the requirements for the degree of

Master of Science

Sabanci University

December 2015

DESIGN AND DEVELOPMENT OF A MICROFLUIDIC DEVICE TO MONITOR IRON  
BINDING DYNAMICS IN IRON TRANSPORT PROTEINS

APPROVED BY:

Prof. Dr. Canan ATILGAN

(Thesis Supervisor)



Prof. Dr. Ali Rana ATILGAN



Prof. Dr. Ali KOŞAR



Prof. Dr. Zehra SAYERS



Assoc. Prof. Dr. Elif ÖZKIRIMLI ÖLMEZ



DATE OF APPROVAL:

29.12.2015

© Gökşin LIU 2015

All Rights Reserved

## ABSTRACT

Iron binding mechanisms of proteins are riveting studies because of the great importance of iron molecules for the metabolism of humans and other organisms. Organisms have developed different mechanisms to catch iron from the environment. Although it is known that this mechanism is rapid and efficient, there is lack of kinetic rate data under different environmental conditions to explain the details of the mechanism.

In this dissertation, a microfluidic device was designed and developed to measure iron binding constants in ferric binding proteins of humans (Transferrin) and bacteria (*Haemophilus Influenzae* Ferric Binding Protein (FBP)), to assess the effect of different environmental conditions on the kinetics of iron – protein association. This study aims to contribute the field by providing a cheap and efficient experimental setup that measures reaction rates of iron binding proteins.

Firstly, a microfluidic chip housing an effective mixing component was designed and fabricated by using PMMA and PDMS as a material. Both designs were tested by using bromocresol green – acetic acid reactions, where the color change from blue to green and from green to yellow can be observed by lowering the pH. The reaction was monitored with high resolution camera. Color changing property of the reaction was used to illustrate total mass transfer in the mixing chamber to determine dead time. Using ANSYS Fluent software these geometries were modified and improved designs were suggested.

Secondly, because the bacterial FBP is not commercially available, it was expressed and purified by using recombinant DNA technology for monitoring iron binding dynamics in the microfluidic device as future work.

## ÖZET

Demir moleküllerinin insan ve diğer organizmaların metabolizması için öneminden dolayı, proteinlerin demir bağlama mekanizması oldukça merak uyandıran bir çalışma konusudur. Organizmalar, bulunduğu çevreden demiri yakalayabilmek için farklı mekanizmalar geliştirmiştir. Bu mekanizmaların çok kolay ve hızlı bir şekilde gerçekleştiği bilinsede, bu reaksiyonların kinetik ölçümleriyle ilgili fazla bilgi bulunmamaktadır.

Bu çalışmada, farklı çevresel koşulların demir – protein kinetiği üzerindeki etkilerini hesaplamak amacıyla, insanlardaki ve bakterilerdeki demir bağlayan proteinlerin (DBP) kinetik sabitlerini ölçebilmek için mikroflüidik bir cihaz tasarlandı ve geliştirildi. Çalışma, demir bağlayan proteinlerin reaksiyon hızlarının ölçerek bu alana katkıda bulunmayı hedeflemiştir.

Öncelikle verimli bir karıştırma kompartmanı içeren mikroflüidik çip, PMMA ve PDMS malzemeleri kullanılarak üretilmiştir. İki tasarımda yeşil bromokresol – asetik asit reaksiyonu ile test edilmiştir. Bu reaksiyon pH değeri düşürüldükçe önce maviden yeşile, daha sonra yeşilden sarıya doğru bir renk değişikliği göstermektedir. Reaksiyon yüksek çözünürlüklü kamera ile kaydedilmiştir. Reaksiyonun bu renk değiştirme özelliği, karıştırma kompartmanında gerçekleşen toplam kütle transferini görüntüleyip, ölü zamanı belirlemek amacıyla kullanılmıştır. ANSYS Fluent programı kullanılarak daha geliştirilmiş geometriler önerilmiştir.

Ayrıca, mikroflüidik cihazda demir bağlama dinamiğinin ölçümlerinde kullanılacak olan bakteriyal DBP ticari olarak satılmadığı için, bu protein rekombinant DNA teknolojisi kullanılarak sentezlenmiş ve saflaştırılmıştır.

*to my beloved family*

*and dearest friends...*

---

*“Scientists investigate that which already is; engineers create that which has never been”*

*Albert Einstein*

## ACKNOWLEDGEMENTS

This dissertation would not have been possible without the help of a huge team of people who often felt challenged but never denied their great support and encouragement along the way.

I would like to express my deepest appreciation to my advisor Prof. Dr. Canan Atilgan for her support, guidance, patience and optimism since the very first day of my graduate education. I would also like to thank to my mentors and committee members; Prof. Dr. Ali Rana Atilgan, Prof. Dr. Ali Koşar, Asst. Prof. Dr. Alpay Taralp, Prof. Dr. Zehra Sayers and Assoc. Prof. Dr. Elif Özkırımlı Ölmez for sharing their suggestions and opinions, helping me to improve my scientific thinking in this process and for the future. I have had a chance to achieve the knowledge I have today thanks to being surrounded by such great minds.

My work on the microfluidic device would not have been completed without İlker Sevgen. His help on this project is tremendous. I would also like to thank him for the motivation and friendship he has provided me during this period. I am also thankful to every member of Koşar's Lab; especially, Abdolali Khalili Sadaghiani, Arzu Özbey, Sarp Akgönül, Buse Balun, Okan Tavoza for sharing their knowledge and experience with me. I would also like to thank Dr. Ines Karmous, Ersoy Çolak for sharing their laboratory practice and skills. I also have the pleasure to extend my gratitude to my group mates, to each and every former visitor or recent member of MIDST Lab.

I am utterly grateful to my friends for their extraordinary patience, support and motivation that made it possible to survive this challenging thesis writing process. I would not have made it without the support of my MAT/BIO Grad friends or MSU friends. I would also like to express my special thanks to Senem Avaz and Utku Seven.

Finally, I would like to extend my deepest gratitude to my beloved family for standing by me with their endless love and patience. I am grateful to my mom, Füzüzan Yılmaz, for encouraging me throughout my life; my dad, Furkan Liu, for supporting my decisions all the time; my uncles who helped me figure out my admiration for science and engineering; and my grandparents for helping me be the person that I am today.

# TABLE OF CONTENTS

CHAPTER I – INTRODUCTION.....	1
CHAPTER II – DESIGN AND DEVELOPMENT OF A MICROFLUIDIC DEVICE TO OBSERVE PROTEIN DYNAMICS BY MONITORING KINETIC DATA .....	10
2.1. BACKGROUND .....	10
2.1.1. Microfluidic Technology .....	10
2.1.2. Materials Used in Microfluidic Devices .....	11
2.1.3. Micromixing .....	15
2.1.4. Simulations .....	16
2.1.4.1. Conservation equations .....	16
2.2. MATERIALS AND METHODS.....	19
2.2.1. Materials .....	19
2.2.1.1. Chemicals .....	19
2.2.1.2. Equipment.....	19
2.2.1.3. Software and Programs.....	19
2.2.1.4. Material Preference of the Microfluidic Chip .....	19
2.2.1.4.1. PMMA – Based Design .....	19
2.2.1.4.2. PDMS – Based Design.....	20
2.2.2. Methods .....	21

2.2.2.1.	Experimental Set Up.....	21
2.2.2.2.	PMMA Microfabrication.....	22
2.2.2.3.	PDMS Microfabrication .....	22
2.2.2.3.1.	Acetate mask design and fabrication.....	22
2.2.2.3.2.	SU-8 Photoresist.....	23
2.2.2.3.3.	Photoresist Coating of Si-Wafer .....	24
2.2.2.3.4.	Soft Lithography .....	25
2.2.2.3.5.	Characterization of SU-8 master.....	26
2.2.2.3.6.	PDMS casting of the SU-8 master .....	26
2.2.2.3.7.	O <sub>2</sub> plasma bonding .....	26
2.2.2.4.	Mixing Analysis Method.....	27
2.3.	RESULTS .....	28
2.3.1.	PMMA .....	28
2.3.2.	PDMS.....	31
2.3.3.	Simulations .....	32
2.3.3.1.	Effect of channel size on mixing effect.....	34
2.3.3.2.	Effect of pin fin distribution on mixing.....	35
2.3.3.3.	Future potential design .....	35
CHAPTER III – EXPRESSION AND PURIFICATION OF <i>HAEMOPHILUS</i>		
<i>INFLUENZAE</i> FERRIC BINDING PROTEIN IN APO-FORM.....		37

3.1.	BACKGROUND .....	37
3.2.	MATERIALS AND METHODS.....	39
3.2.1.	Materials .....	39
3.2.1.1.	Chemicals .....	39
3.2.1.2.	Equipment.....	39
3.2.1.3.	Software and Programs.....	39
3.2.2.	Methods .....	39
3.2.2.1.	Preparation of LB Growth Media.....	39
3.2.2.2.	Preparation Buffers and Solutions.....	39
3.2.2.3.	Construction of pET-28a (+) containing Ferric Binding Protein encoding gene	41
3.2.2.4.	Preparation of component cells: .....	42
3.2.2.5.	Transformation of the engineered pET-28a (+) into TOP10 and BL21:.	43
3.2.2.6.	Isolation of plasmid DNA .....	44
3.2.2.7.	Digestion of the plasmid with restriction enzymes NdeI and XhoI .....	44
3.2.2.8.	Confirmation with agarose gel electrophoresis .....	45
3.2.2.9.	Expression of FBP in BL21 cells .....	46
3.2.2.10.	Purification of Ferric Binding Protein.....	46
3.2.2.10.1.	Lysis of the cells by BugBuster protocol .....	46
3.2.2.10.2.	Ni-affinity column purification of FBP.....	47

3.2.2.11. SDS-Page check .....	47
3.2.2.12. Dialysis of the FBP to remove imidazole .....	48
3.2.2.13. Removing Fe <sup>+3</sup> ions from holo-FBP .....	48
3.2.2.14. Concentration of the apo-FBP.....	49
3.2.2.15. Preparation of FeCl <sub>3</sub> solutions .....	49
3.2.2.16. Bradford assays .....	50
3.3. RESULTS:.....	50
3.3.1. Construction of pET-28a (+) containing FBP encoding gene .....	50
3.3.2. Transformation of the engineered pET-28a (+) into TOP10 and BL21 .....	52
3.3.3. Confirmation with agarose gel electrophoresis .....	52
3.3.4. Control of protein expression in E. coli with SDS-page analysis.....	53
3.3.5. Concentration of the protein solution .....	54
CHAPTER IV – DISCUSSION .....	57
4.1. Design and Development of the Microfluidic Device .....	57
4.2. Expression and Purification of the FBP.....	58
CHAPTER V – CONCLUSION AND FUTURE WORK .....	59
5.1. Conclusions.....	59
5.2. Future Work.....	60
BIBLIOGRAPHY .....	62

APPENDIX A.....	66
APPENDIX B.....	69

## LIST OF FIGURES

Figure 1: Crystal structure of Transferrin in 2.7 Å resolution at physiological pH. Two lobes are located on the right and left connected with a linker (gray). Each subunit is colored in different color. (PDB 1BP5).....	1
Figure 2: (a) Transferrin keeps an iron in each lobe. (b) Amino acid coordination to hold iron. ....	2
Figure 3: Endocytic cycle of transferrin (adapted from reference [9]).....	3
Figure 4: Iron acquisition from transferrin to Haemophilus Influenzae ferric binding protein (adapted from ref. [14]) .....	4
Figure 5: (a) Bacterial FBP holds only one iron. (b) Amino acid coordination to keep iron .5	
Figure 6: Reduction of 2,6-dichlorophenolindopheno (DICP) by ascorbic acid. Reaction rate was calculated for different ascorbic acid concentrations. Second graph is the linearized curves with 9 ms of dead time shown with dashed line. (Adopted from ref. [17])7	
Figure 7: Fluorescence intensity was measured for the reaction of HDAH with fluorescamine (Adopted from ref. [17]) .....	8
Figure 8: Chemical structure of PDMS, where $n$ is the number of the repeating monomers. Typically, $n$ is accepted as ~60 in PDMS oligomers.....	<b>Error! Bookmark not defined.</b>
Figure 9: A catalyst containing Platinum causes cross-linking between PDMS oligomers and leads to polymerization. ....	<b>Error! Bookmark not defined.</b>
Figure 10: Fabrication of the master by photo lithography. (Adopted from ref. [20]).....	13
Figure 11: Master is used for PDMS casting. This procedure can be completed in 24 hours (Adopted from ref. [18]) .....	14

Figure 12: Technical drawing of PMMA microfluidic chip for microfabrication. ....	20
Figure 13: Adjusted dimensions of microfluidic devices for PDMS fabrication. ....	21
Figure 14: Photomask design to print on to transparency with high resolution. ....	23
Figure 15: The speed of the rotation and spinning time was determined by MicroChem Company. ....	24
Figure 16: At constant flow rate, the distance of the fluid traveled is proportional to time. ....	28
Figure 17: The time is calculated by calibration of the mixing chamber by distance and flow rate. ....	29
Figure 18: The flow was recorded at $Q = 5$ ml/min. ....	29
Figure 19: The flow was recorded at $Q = 10$ ml/min. ....	30
Figure 20: The flow was recorded at $Q = 13$ ml/min. ....	30
Figure 21: Time was calculated as a function of distance. ....	31
Figure 22: The flow caption at $Q=500$ $\mu$ l/min in PDMS design. ....	32
Figure 23: The schematic computational domain identified to program: (a) shows the microchannels in microfluidic chip, (b) shows only the mixing chamber. ....	33
Figure 24: Numerical analysis of micromixing channel geometry with pin-fins at flow rate $Q=10$ ml/min. ....	34
Figure 25: Effect of channel size on mixing phenomena. The scale on the right represents the channel size. (a) displays a channel with a width of 2 mm whereas, (b) displays a channel double the size of a. ....	35
Figure 26: Effect of pin-fin distribution on mixing. ....	35
Figure 27: Potential future design at $Q=0.3$ ml/min. ....	36

Figure 28: pET-28a(+) vector with T7 promoter, kanamycin resistance gene, NdeI and XhoI restriction sites .....51

Figure 29: FBP coding gene sequence with His-tag and TEV site at the beginning and a stop codon at the end. ....51

Figure 30: Constructed FBP coding gene was inserted in between restriction sites NdeI and XhoI. ....52

Figure 31: (a) Agarose gel confirmation of TOP10 cells. (b) Agarose gel confirmation of BL21 cells.....53

Figure 32: SDS-Page control of the protein. PL: pellet, S: supernatant, FT: flow through, W: washing, E: elution.....54

Figure 33: Protein concentration after dialysis .....**Error! Bookmark not defined.**

Figure 34: Protein concentration after the separation of iron**Error! Bookmark not defined.**

Figure 35: Increased concentration .....**Error! Bookmark not defined.**

Figure 36: Expected color gradient.....60

Figure 37: Optical detection compartment (adapted from ref. [17]) .....61

## LIST OF TABLES

Table 1: Chemical and mechanical properties of PMMA and PDMS.....	11
Table 2: All the process details are given by the MicroChem Company depending on the thickness.....	25
Table 3: Physical properties of bromocresol green and acetic acid at room temperature ....	33
Table 4: Concentrations of TOP10 and BL21 cells after transformation .....	44
Table 5: Digestion of the plasmid from the restriction sites to cut the gene .....	45
Table 6: Stock FeCl <sub>3</sub> solution was diluted into various concentrations .....	49

## LIST OF ABBREVIATIONS

CAD	Computer Aided Design
CD	Circular Dichroism
CO <sub>3</sub> <sup>-2</sup>	Carbonate
CSF	Continuum Surface Force
DBP	Demir Bağlayan Protein
DICP	2,6-dichlorophenolindophenol
DNA	Deoxyribonucleic Acid
<i>E.coli</i>	<i>Escherichia coli</i>
FBP	Ferric Binding Protein
FbpA	<i>Haemophilus Influenzae</i> Ferric Binding Protein
FbpC	<i>Haemophilus Influenzae</i> ATP Binding Protein
Fe <sup>+3</sup>	Iron (III)
FVM	Finite Volume Method
H <sub>2</sub> PO <sub>4</sub>	Phosphate
HDAH	histone deacetylase like amidohydrolase
His-Tag	Histidine Tag
IPTG	isopropyl-beta-D-thiogalactopyranoside
KAN	Kanamycin

OD	Optical Density
PDMS	Polydimethylsiloxane
PEB	Post Exposure Baking
PMMA	Poly (methyl methacrylate)
Re	Reynolds Number
SDS-PAGE	Sodium Dodecyl Sulfate Polyacrylamide Gel Electrophoresis
Si-OH	Silanol Group
TAE	Tris-Acetate-EDTA Buffer
TEV	Tobacco Etch Virus
TFR	Transferrin
$T_G$	Glass transition temperature
UDF	User Defined Function
UV	Ultra Violet
VOF	Volume of Fluid

## CHAPTER I – INTRODUCTION

Iron is an essential molecule for all the biological systems, functioning in complex mechanisms as both an electron donor and an acceptor for metabolism [1]. For instance, its ability to carry oxygen makes it crucial for mammalian cells whereas, in Gram-negative bacteria ferric ions are responsible of other vital processes [2]. Mammals are capable of receiving iron from the nutritional supplements, whereas bacteria have developed their own strategy to hijack iron from host organisms [3], [4], [5].

In human cells, transferrin is the responsible protein of catching iron ions in the blood and delivering them to the cell. It is synthesized in the liver, and then released into the plasma. The structure of the protein contains two lobes and a linker in between. During the iron binding mechanism, the two lobes bend onto each other and the linker behaves like a hinge. Each lobe has two subunits (Figure 1).

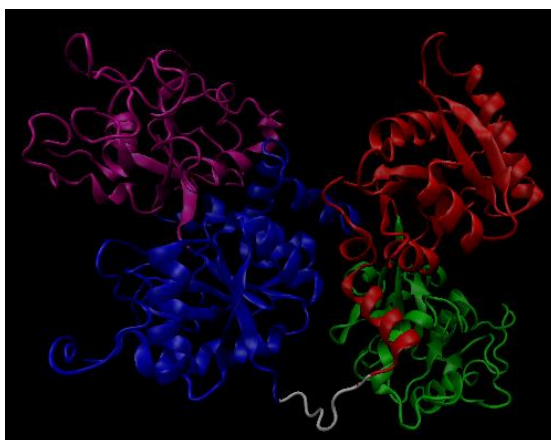


**Figure 1: Crystal structure of Transferrin in 2.7 Å resolution at physiological pH. Two lobes are located on the right and left connected with a linker (gray). Each subunit is colored in different color. (PDB 1BP5)**

In each lobe, an iron ( $\text{Fe}^{+3}$ ) can be carried coupled with a carbonate ion ( $\text{CO}_3^{-2}$ ). Carbonate becomes a synergistic anion in this mechanism [6]. On the other hand, there are

four highly conserved amino acids in the structure responsible from holding this complex in the protein (Figure 2) [7]. Those residues are indicated as an aspartic acid (D63), two tyrosine residues (Y95 and Y118) and a histidine residue (H249). Another arginine residue (R124) stabilizes the synergistic anion [8]. Binding of the iron causes a large conformational change on the structure by opening the lobes and twisting them. Transferrin protein can be found in the apo, mono-ferric or di-ferric conformations depending on the number of iron it is carrying.

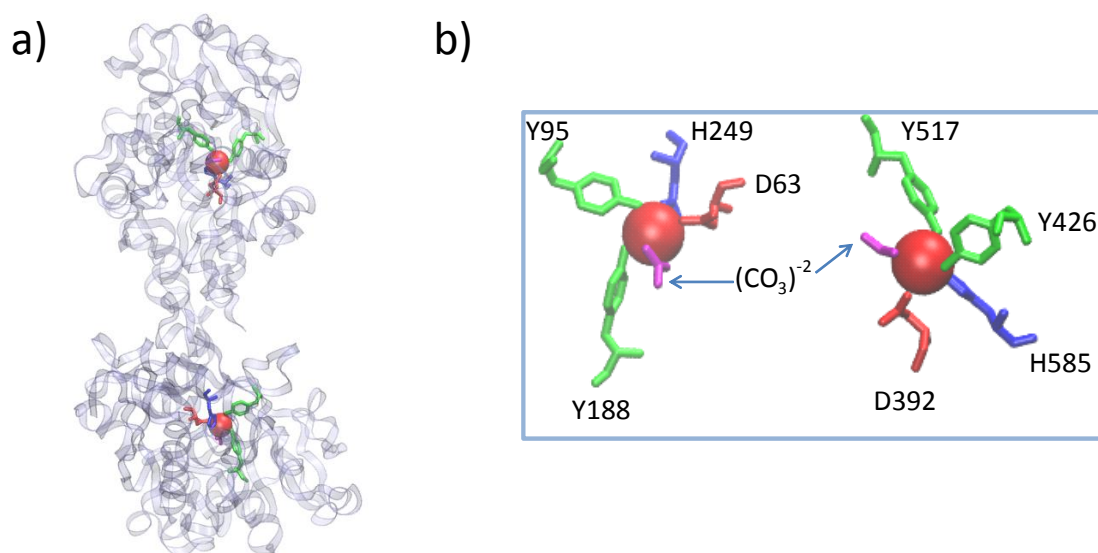


**Figure 2: (a) Transferrin keeps an iron in each lobe. (b) Amino acid coordination to hold iron.**

The iron transferrin mechanism is derived by pH dependency. Once the iron is kept by the protein, it flows through the blood until it finds a receptor specific to transferrin (TFR) on the cell surface. The salt bridge formed between D240 and R678 in the structure is thought to be the reason of the transferrin's selectivity to the transferrin receptor [8]. Iron bounded transferrin binds to TFR on the cell surface at pH 7.4 in the endocytic cycle. This transferrin – TFR complex is endocytosed. Transferrin releases iron in the endosome, when the pH is lowered down to 5.6.  $Fe^{+3}$  is reduced to  $Fe^{+2}$  in the endosome. Now, the  $Fe^{+2}$  can be carried out of the cell by the divalent metal transporter. Transferrin turns into apo form again and remains as a complex with TFR at pH 5.6. Then, it is recycled back to the cell

surface. Elevated pH causes apo transferrin to be detached from the TFR, thus leading to its ability to capture more  $\text{Fe}^{+3}$  Figure 3 [9].

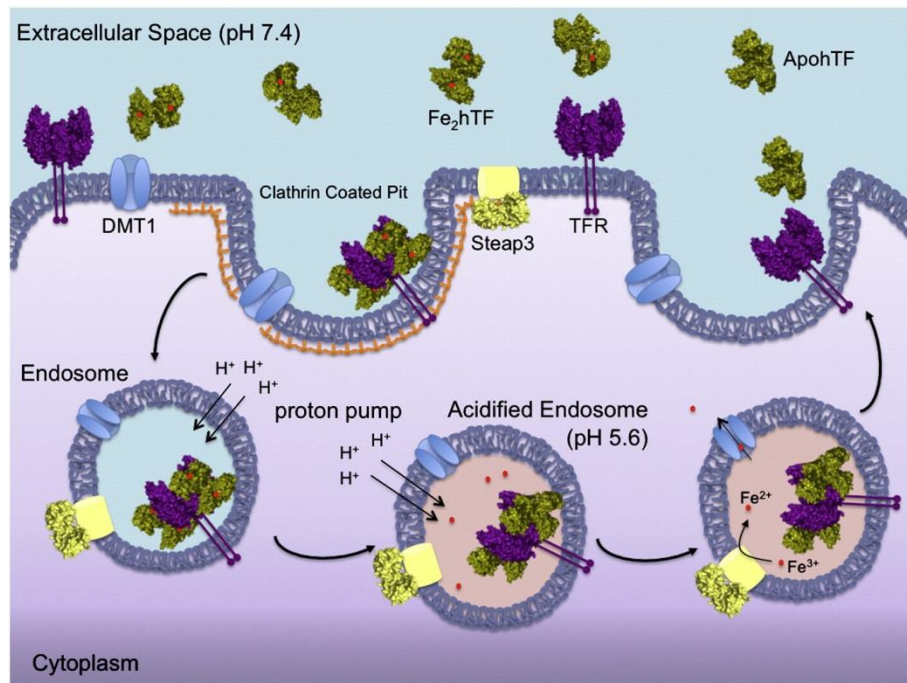


**Figure 3: Endocytic cycle of transferrin (adapted from reference [9])**

The overall mechanism has been studied experimentally for over 30 years. The association constant for iron binding the transferrin protein was measured approximately as  $10^{22} \text{ M}^{-1}$  at physiological pH, showing that it is a very probable and fast process with high affinity [10]. Moreover, binding of transferrin to transferrin receptor is another significant process for the mechanism. The studies showed that the diferric transferrin binds to the receptor with a greater affinity than the monoferric or apo transferrin. Association constant of diferric transferrin is around  $10^9 \text{ M}^{-1}$ ; whereas, association constant of monoferric form of transferrin is about  $10^6 \text{ M}^{-1}$  [11]. As a result, diferric form of the transferrin is more probable to bind to a receptor in order to release its iron into the cell. Given association constants can be interpreted as that binding of iron to protein is a reaction overpasses the activation energy barrier easily under physiological conditions. Therefore, it can be

assumed that those reactions happen very fast, despite the lack of reaction rate information in the literature.

On the other hand, ferric binding protein (FBP) of pathogenic Gram – negative bacteria also has high affinity to  $\text{Fe}^{+3}$  ions, causing iron takeover from human metabolism and following iron deficiency related diseases [12]. Similar to iron binding mechanism of it, bacterial FBP is also part of the highly developed iron acquisition system from the host.

Ferric binding protein from *Haemophilus Influenzae* has been well-studied in order to understand iron hijacking mechanism of the pathogenic bacteria [13]. Iron acquisition from transferrin to pathogenic bacterial protein is described in Figure 4. Transferrin of the host organism is captured by a receptor called TbpB, located on the bacterial surface. In this position, the iron is detached from transferrin and transported to the periplasmic space of the Gram-negative bacteria. Here, iron is captured by the ferric binding protein (FbpA). With the help of ATP binding protein (FbpC), the iron is transported to the inner membrane [14].

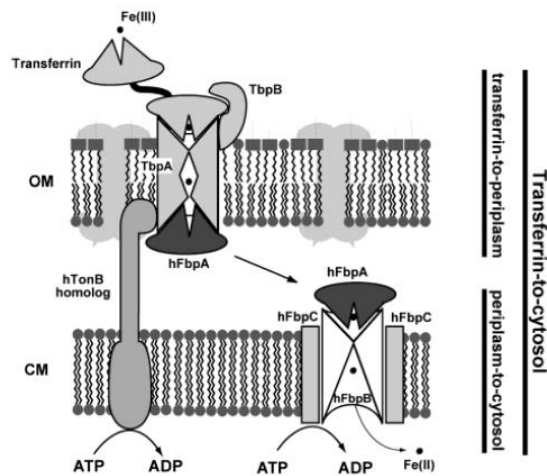


**Figure 4: Iron acquisition from transferrin to *Haemophilus Influenzae* ferric binding protein (adapted from ref. [14])**

Unlike human transferrin, bacterial FBP can host only one ferric ion. Conserved amino acids responsible of holding iron are shown in Figure 5 [15]. The N – terminal domain of the protein recognizes the iron and encloses on top of the C – terminal domain. Phosphate ( $\text{H}_2\text{PO}_4^-$ ) molecule is the synergistic anion in this mechanism. The presence of this synergistic anion increases the affinity of the protein from  $K_a$  value of  $4.3 \times 10^2 \text{ M}$  to  $2.4 \times 10^{18} \text{ M}$ . The iron is coordinated in the protein with Y195, Y196, E57 and H9 residues with the help of synergistic anion [14], [15].

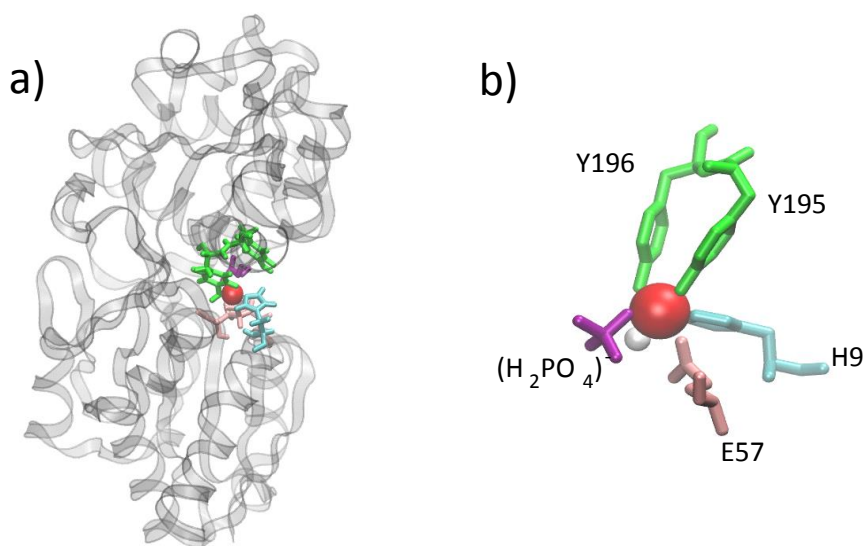


**Figure 5: (a) Bacterial FBP holds only one iron. (b) Amino acid coordination to keep iron**

If the coordinated amino acid regions of transferrin and FBP holding the iron are compared, the resemblance of these conserved regions can be observed. In particular, existence of synergetic anions in both human transferrin and bacterial FBP is accepted as proof of convergent evolution [16].

In this thesis, we aim to design a microfluidic device to measure iron binding/release constants of ferric binding proteins existing in human (Transferrin) and bacteria (*Haemophilus Influenzae* Ferric Binding Protein), in order to assess the effect of different environmental conditions on the kinetics of iron – protein association. Since the comparable commercial designs are very expensive, cost efficiency of our design has great

significance. In addition, because the reaction rate data lack in the literature for iron binding to particular proteins, designing such a device to make simple reaction rate measurements is also innovative.

Microfluidic technology is a flourishing innovation in many fields, considering the ease of fabrication, low costs and low sample volumes to be consumed. Furthermore, it is a leading preference when it comes to monitor fast reactions. The main objective of our design is to measure fast biochemical reactions arising on millisecond time scale in different environmental conditions at low cost. Miniaturization of such systems down to micro scales enables monitoring reactions within small volumes. Therefore, the compactness of the design is one of the most important aspects. Efficient mixing is required in such designs, because the reaction time can be measured after the reactants are thoroughly exposed to each other. Consequently, micromixing technology used in the design becomes one of our major focal points. On the other hand, disposability of the materials, which are in direct contact with the chemicals or other samples, is another significant aspect of our design. Considering the ease of fabrication and inexpensive materials, disposability is another of our main purposes to avoid contamination and errors.

In consideration of all these aspects, we built and tested microfluidic device with different designs, aiming a better performance to monitor fast reactions, iron binding kinetics in our case. Our work was inspired by the study of Bleul et al. [17].

Our purpose by developing this microfluidic device is to be able to get an absorbance curve to follow the kinetics of the reaction. The reference study has tested their design by monitoring a first order reaction, reduction of 2,6-dichlorophenolindophenol (DICP) by ascorbic acid [17]. Figure 6 shows results for this specific reaction, where the dead time of the design was also determined.

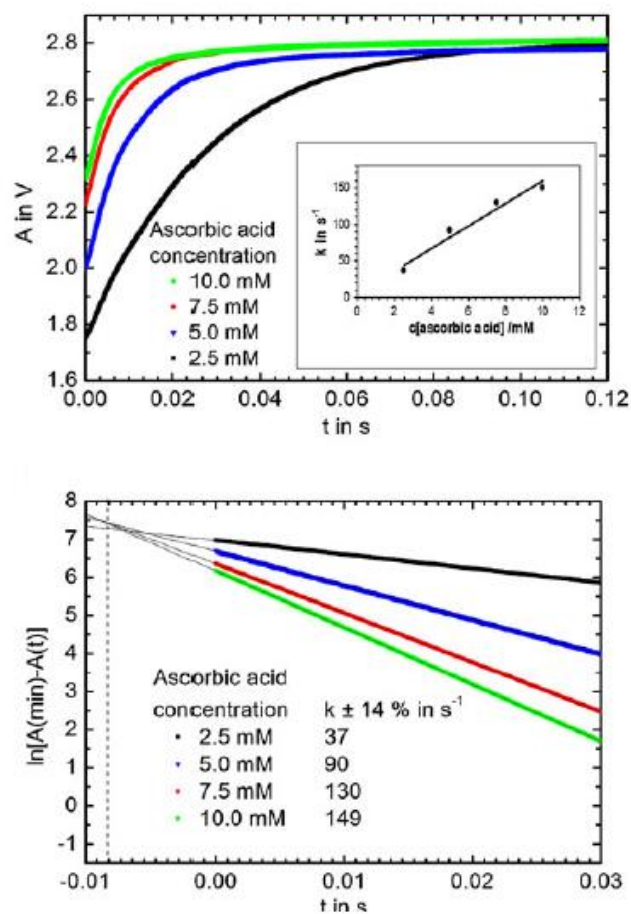


**Figure 6: Reduction of 2,6-dichlorophenolindopheno (DICP) by ascorbic acid. Reaction rate was calculated for different ascorbic acid concentrations. Second graph is the linearized curves with 9 ms of dead time shown with dashed line. (Adopted from ref. [17])**

That the time scales relevant to protein binding kinetics may be accessed by such a device was also demonstrated therein, by labeling of histone deacetylase like amidohydrolase (HDAH) with fluorescamine. The rate constants for this two-step reaction on the order of  $100 \text{ s}^{-1}$  were correctly determined (Figure 7) [17].

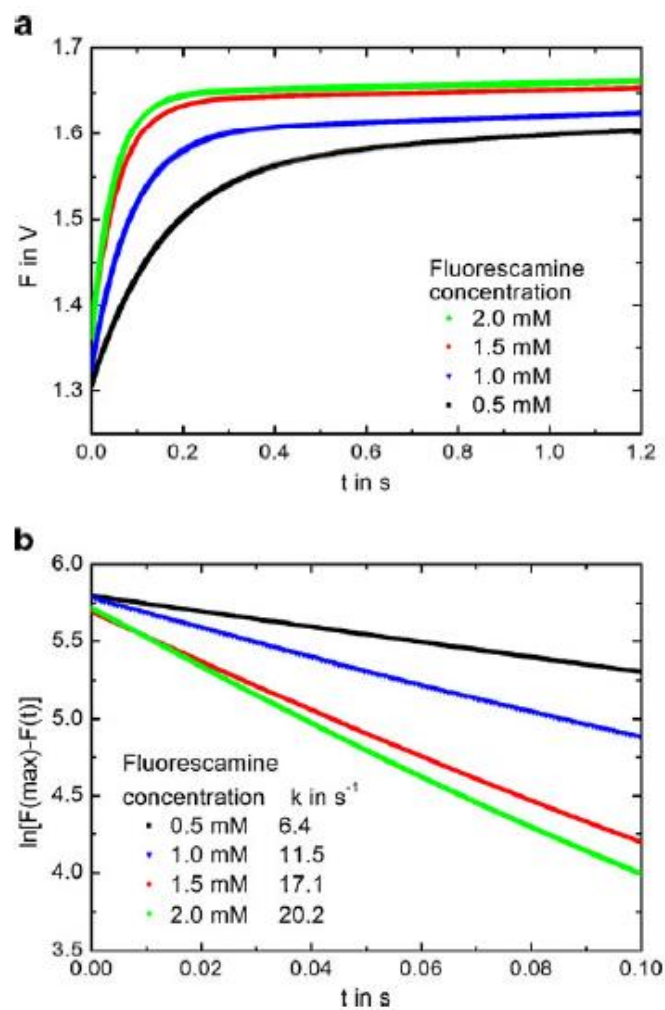


Figure 7: Fluorescence intensity was measured for the reaction of HDAH with fluorescamine (Adopted from ref. [17])

This thesis mostly focuses on designing a microfluidic system with efficient mixing to obtain reduced dead times of the reactions. The system was evaluated by monitoring the reaction between bromocresol green and acetic acid. Because acid and indicator reacts much faster than the overall mass transfer, meaning diffusion of two flows in the mixing area, we presumed it would serve as a good model to accurately illustrate the mixing time. This procedure is clarified in Chapter II. Additionally, Haemophilus Influenzae ferric binding protein was expressed in apo form using recombinant techniques. Chapter III is devoted to the expression and characterization of the protein. Difficulties, limitations and advantages of the study are discussed in Chapter IV whereas; Conclusions and Future Work are described in Chapter V.

## **CHAPTER II – DESIGN AND DEVELOPMENT OF A MICROFLUIDIC DEVICE TO OBSERVE PROTEIN DYNAMICS BY MONITORING KINETIC DATA**

### **2.1. BACKGROUND**

#### **2.1.1. Microfluidic Technology**

Microfluidics is a demanding, developing technology due to its wide range of application areas. Field of microfluidics comprises medical and environmental application, in addition to chemistry, biochemistry, biology. Miniaturization of the systems down to the micro scale enables observation of the fast reactions in higher resolution on the time scale of milliseconds, while reducing the consumption of sample volumes [18]. Therefore, with this system it is possible to monitor biochemical reactions such as protein-ligand interactions. A typical microfluidic system has side-by-side dimensions of 10 – 1000  $\mu\text{m}$  to manipulate  $10^{-9}$  to  $10^{-18}$  liters of fluid in the area [18]. The advantages of using a microfluidic system includes consumption of minimized amounts of sample, toxic or explosive chemicals, reduced cost in fabrication, therefore easy disposal, decreased amount of risky by-products and reduced of analysis time[19].

Designing of a microfluidic system primarily requires a clear perspective of the expected components. These systems can be used for mixing, separation, injection, detection or treatment [20]. These components then affect the material and fabrication preferences. The choice of material is important for the movement of the fluid in the channels. Smoothness of the surface, machinability, transparency, bioavailability and chemical and mechanical stability of the material are the most important properties of material choice. In these terms, Poly (methyl methacrylate) (PMMA; Plexiglas<sup>®</sup>) and Polydimethylsiloxane (PDMS) are popular polymers to be used in microfluidic devices.

### 2.1.2. Materials Used in Microfluidic Devices

Poly (methyl methacrylate) is a transparent thermoplastic with a chemical composition of  $(C_5O_2H_8)_n$ . The transparency and machinability of the material is an important reason why it is used in microfluidic systems. The mechanical and chemical properties of PMMA are listed in the Table 1.

**Table 1: Chemical and mechanical properties of PMMA and PDMS. [18], [21], [22], [23], [24].**

Property	PMMA	PDMS
Optical	Optical absorption at 190 nm.	Optical absorption at 240 nm.
Mass density	1.18 kg/m <sup>3</sup>	0.97 kg/m <sup>3</sup>
Young's modulus	1800 – 3100 MPa	360 – 870 KPa
Specific heat	1.46 kJ/kg.K	1.46 kJ/kg.K
Glass transition temperature ( $T_G$ )	105°C	-123°C
Melting point	160°C	-50°C
Thermal conductivity	0.15 W/m.K	0.167 – 0.25 W/m.K
Biocompatibility	Bioavailable, nontoxic	Mostly bioavailable; toxic by time
Hydrophobicity	Hydrophobic; contact angle: 72°	Highly hydrophobic; contact angle: 90° - 120°

Polydimethylsiloxane (PDMS) is the preferred polymer because of its optical transparency, ease of fabrication, bioavailability, nontoxicity and surface chemistry in microfluidic devices. It is a silicon based oligomer which becomes a chemically and thermally stable polymer after it is cured. The physical and chemical properties of the material are listed in Table 1 [18], [21], [22], [23], [24].

The stability of the oligomer is provided by polymerization. The chemical formula of PDMS is  $\text{CH}_3[\text{Si}(\text{CH}_3)_2\text{O}]_n\text{Si}(\text{CH}_3)_3$ , where  $n$  is the number of repeating dimethylsilanol monomeric units (Figure 8). Platinum catalyzes the reaction via oxidative addition and reductive elimination mechanism, and this causes branching of the oligomers from the vinyl ends of ethoxy-dimethyl vinyl-silane groups; yielding cross – linking [25]. By additional of heat curing, PDMS fully polymerizes. The chemical reaction is illustrated in the Figure 9.

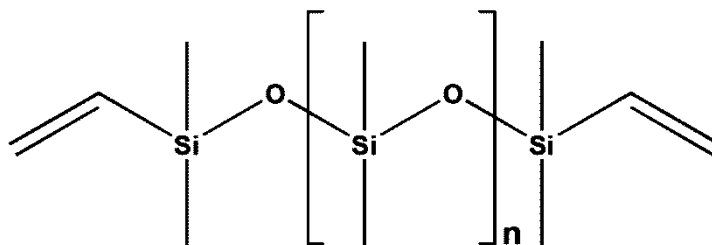


**Figure 8: Chemical structure of PDMS, where  $n$  is the number of the repeating monomers. Typically,  $n$  is accepted as ~60 in PDMS oligomers..**

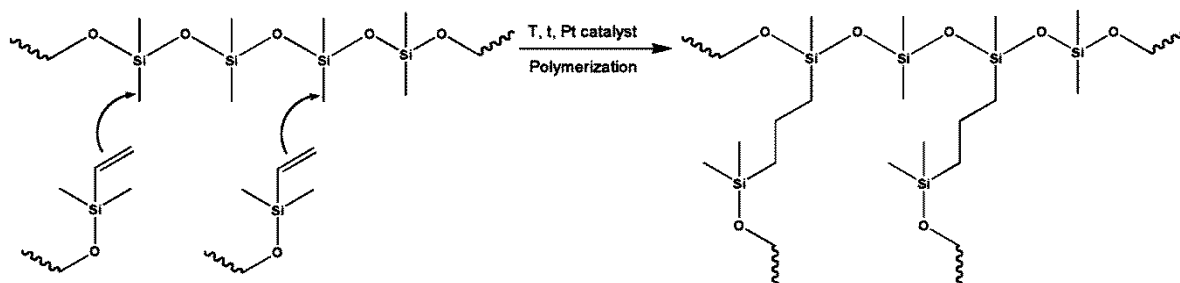


**Figure 9: A catalyst containing Platinum causes cross-linking between PDMS oligomers and leads to polymerization.**

Ease of fabrication of PDMS is the major advantage. It is possible to fabricate a PDMS microfluidic chip in 24 hours. The first step is to produce a master for casting of PDMS. The prototype device is drawn in a computer aided design (CAD) program, and printed on a transparent sheet at high resolution. In the photolithography step, the transparency is used to produce photoresist on the silicon wafer. The process master fabrication is shown in the Figure 10 [20].

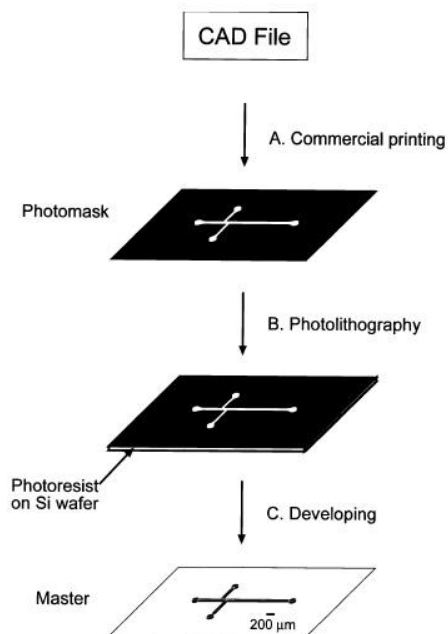


**Figure 10: Fabrication of the master by photo lithography. (Adopted from ref. [20])**

For the fabrication of the master mold, silicon wafer is homogeneously coated with an epoxy-based photoresist called SU-8. This material is polymerized under the UV light and it composes a rigid body. SU-8 coated wafer and the photomask of the prototype is located in the lithography machine and exposed to UV light. Therefore, the light passing through the transparency reaches to the SU-8 coated wafer and causes hardening in these areas. The regions that are not exposed to UV light remain liquid and can be washed with developer. Consequently, a negative master for PDMS casting is generated on the wafer. PDMS is easy to remove from the master without any damage, because of its low surface

free energy and elasticity. The master mold can be used until it is broken as a result of a human error. The process is demonstrated in Figure 11 [18].

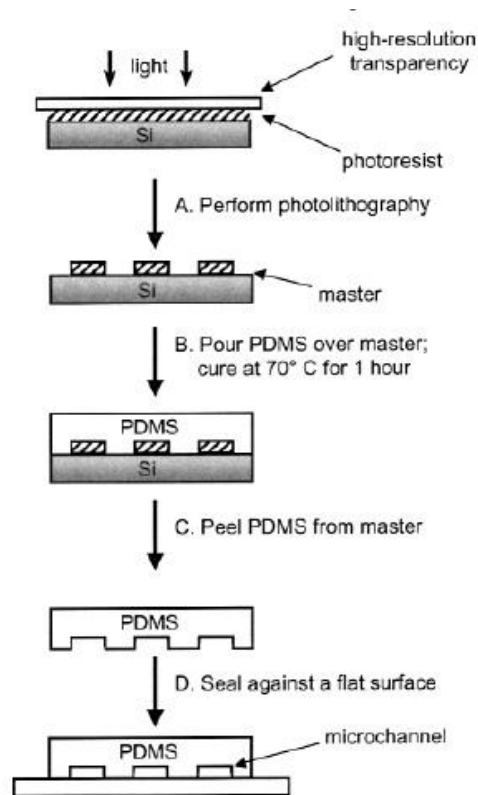


**Figure 11: Master is used for PDMS casting. This procedure can be completed in 24 hours (Adopted from ref. [18])**

Micro channels can be sealed by performing air plasma on the surfaces. With this method, the methyl ends of the PDMS are introduced with silanol groups (Si-OH). Glass can be used to seal PDMS. Glass surface is put into contact with PDMS with open silanol groups after the glass surface is also exposed to air plasma. Si-O-Si bonds are made between PDMS and glass surface.

### **2.1.3. Micromixing**

Micromixing is the most crucial step in microfluidic systems. In particular, biochemical applications of the devices require an efficient mixing. Mechanical properties of fluids are important for the design of the mixing compartment. The theory of fluid mechanics on the macro scale can be applied to micro environments.

The characteristic of a fluid flow is determined with its Reynolds Number (Re). Low Re number is named as laminar flow, where the motion of the fluid is smooth and constant. However, with higher Re number the flow can cause vortices and fluctuations; therefore it is called turbulent flow [26]. Generally, microfluidic systems have low Re numbers. Therefore, they usually have laminar flow, where the flow goes parallel to each other with a constant velocity with respect to time and location. Hence, the mass transfer occurs only in one direction and mixing can be obtained through diffusion.

In order to reach higher Re numbers in microenvironments, micromixers are used to change the inertial forces affecting the fluid. Random motion is targeted in these systems to achieve a convective mass transport in all directions [27]. Different channel geometries provide an effective mixing in microsystems by increasing the contact surface area and decreasing the mixing path [26]. Benefiting from micro pin-fins for maximizing the contact surface in order to get better mixing has been very successful [28].

In this study, effective mixing was required to determine more accurate iron binding kinetic rate data for proteins. Efficiency was evaluated by using the color change of bromocresol green and acetic acid reaction as a probe to monitor mixing time. As follows, simulations of mixing were done to improve the system designs.

#### 2.1.4. Simulations

The flow can be simulated with different numerical methods in order to estimate characteristic of the stream and its mixing properties. Mathematical statement of the flow is used to calculate consequences of various parameters such as geometry, flow rate, type of the fluids, etc. Numerical methods are inexpensive, handy and flexible analysis of the microfluidic systems.

In the field of computational fluid dynamics, Finite Volume Method (FVM) is one of the several powerful discretization methods. FVM is composed of two steps; first is where the numerical domain is partitioned into a set of control volumes, while the second deals with the integration of the differential form of the governing equations over each control volume. Thereafter, interpolation profiles are assumed to describe the variation of the corresponding variable to give the discretized or discretization equation. Thus, the conservation principle is expressed inside the control volume so that the resulting solution meets the conservation of quantities, such as mass or momentum. This holds for each control volume along with the full computational domain for any number of control volumes.

The theory behind the analysis relies on numerical equations depending on the number of the phases, physical properties of the fluids and geometry of the mixing chamber. All the numerical definitions are justified based on fundamentals of physics; conservation of the mass and conservation of momentum.

##### 2.1.4.1. Conservation equations

The conservation of mass for two phases is described by equation 1. Tracing of the interface is achieved by the solution of a continuity equation for the volume fraction of one (or more) of the phases.

$$\frac{1}{\rho_q} \left[ \frac{\partial}{\partial t} (\alpha_q \rho_q) + \nabla \cdot (\alpha_q \rho_q \bar{v}_q) \right] = S_q + \sum_{p=1}^n (\dot{m}_{pq} - \dot{m}_{qp}) \quad (1)$$

where  $\dot{m}_{pq}$  is the mass transfer from phase  $p$  to phase  $q$ , and  $\dot{m}_{qp}$  is the mass transfer from phase  $q$  to phase  $p$ . In this equation,  $S_q$  is the source term, which, in our case, is equal to zero. The primary-phase volume fraction is computed based on the following constant:

$$\sum_{q=1}^n \alpha_q = 1 \quad (2)$$

The properties of materials are involved in the equation by averaging the volume fractions of the densities.

The law of the conservation of momentum is represented in the analysis by integrating equation 2, which depends on the volume fractions of all phases through the properties  $\rho$  and  $\mu$ .

$$\frac{\partial}{\partial t} (\rho \bar{v}) + \nabla \cdot (\rho \bar{v} \bar{v}) = -\nabla p + \nabla \cdot [\mu (\nabla \bar{v} + \nabla \bar{v}^T)] + \rho \bar{g} + \bar{F} \quad (4)$$

The VOF model can also include the effects of surface tension along the interface between each pair of phases. The model can be augmented by the additional specification of the contact angles between the phases and the walls. One can specify a surface tension coefficient as a constant, as a function of temperature, or through a User Defined Function (UDF). The solver includes the additional tangential stress terms (causing what is termed as Marangoni convection) that arise due to the variation in surface tension coefficient. Variable surface tension coefficient effects are usually important only in zero/near-zero gravity conditions, which are not operating in our systems.

Surface tension arises as a result of attractive forces between molecules in a fluid. If we consider an air bubble in water, the net force on a molecule due to its neighbors is zero within the bubble. At the surface, however, the net force is radially inward, and the combined effect of the radial components of force across the entire spherical surface is to

make the surface contract, thereby increasing the pressure on the concave side of the surface. The surface tension is the force acting only at the surface that is required to maintain equilibrium. It acts to balance the radially inward inter-molecular attractive force with the radially outward pressure gradient force across the surface. In regions where two fluids are separated, but one of them is not in the form of spherical bubbles, the surface tension acts to minimize free energy by decreasing the area of the interface.

The surface tension model in FLUENT is the continuum surface force (CSF) model proposed by Brackbill et al. [29]. With this model, the addition of surface tension to the VOF calculation results in a source term in the momentum equation. To understand the origin of the source term, consider the special case where the surface tension is constant along the surface, and where only the forces normal to the interface are considered. It can be shown that the pressure drop across the surface depends upon the surface tension coefficient,  $\sigma$ , and the surface curvature as measured by two radii in orthogonal directions,  $R_1$  and  $R_2$ :

$$P_1 - P_2 = \sigma \left( \frac{1}{R_1} + \frac{1}{R_2} \right) \quad (5)$$

Here,  $P_1$  and  $P_2$  are the pressures in the two fluids on either side of the interface.

In FLUENT, a formulation of the CSF model is used, where the surface curvature is computed from local gradients in the surface normal at the interface. Let  $n$  be the surface normal, defined as the gradient of  $\alpha_q$ , the volume fraction of the  $q^{th}$  phase,  $n = \nabla \alpha_q$ . The curvature,  $\kappa$ , is defined in terms of the divergence of the unit normal,  $\hat{n}$  [29]:

$$\kappa = \nabla \cdot \hat{n}, \text{ Where; } \hat{n} = \frac{n}{|n|}.$$

## **2.2. MATERIALS AND METHODS**

### **2.2.1. Materials**

#### **2.2.1.1. Chemicals**

Chemicals used in the study are listed in the Appendix A.

#### **2.2.1.2. Equipment**

Equipment used in the study are listed in the Appendix B.

#### **2.2.1.3. Software and Programs**

Solidworks

ANSYS Fluent

#### **2.2.1.4. Material Preference of the Microfluidic Chip**

Material preference was one of the most critical aspects of the design. Considering the features such as transparency of the material, durability against high flow rates, surface properties, chemical resistance to different pH values, ease of fabrication and machinability, disposability and cost of the material, two different materials were decided to be used for microchip fabrication.

- PMMA: Poly (methyl methacrylate), commercially known as Plexiglas.
- PDMS: Polydimethylsiloxane

##### **2.2.1.4.1. PMMA – Based Design**

The microchip was designed by using SolidWorks. The dimensions are shown in the 2D drawing in Figure 12. The outer dimensions of the design were determined as 43 mm x 99 mm, based on reference article [17]. At the entrance, micro channels were designed with 0.4 mm width and 0.5 mm depth. Mixing chamber was planned to be the first place where the reactants were met. 15 diamond shaped fins were placed along the 16 mm

long, 2.5 mm wide mixing chamber. The depth of the mixing channel was planned to be 0.5 mm.

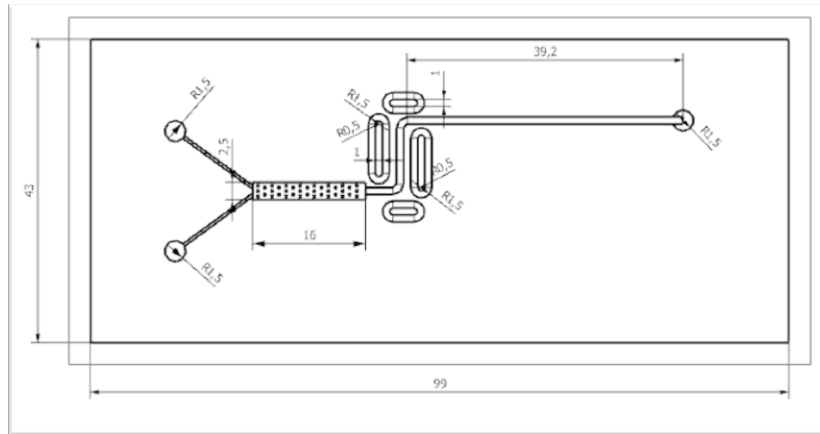


**Figure 12: Technical drawing of PMMA microfluidic chip for microfabrication.**

#### **2.2.1.4.2. PDMS – Based Design**

The dimensions of the design were adjusted for the fabrication of the PDMS microfluidic chip. Because of the limitations of the fabrication process, micro channels and mixing chamber were modified so that the minimum distance between the two walls is 125  $\mu\text{m}$ . The final design is displayed in Figure 13.

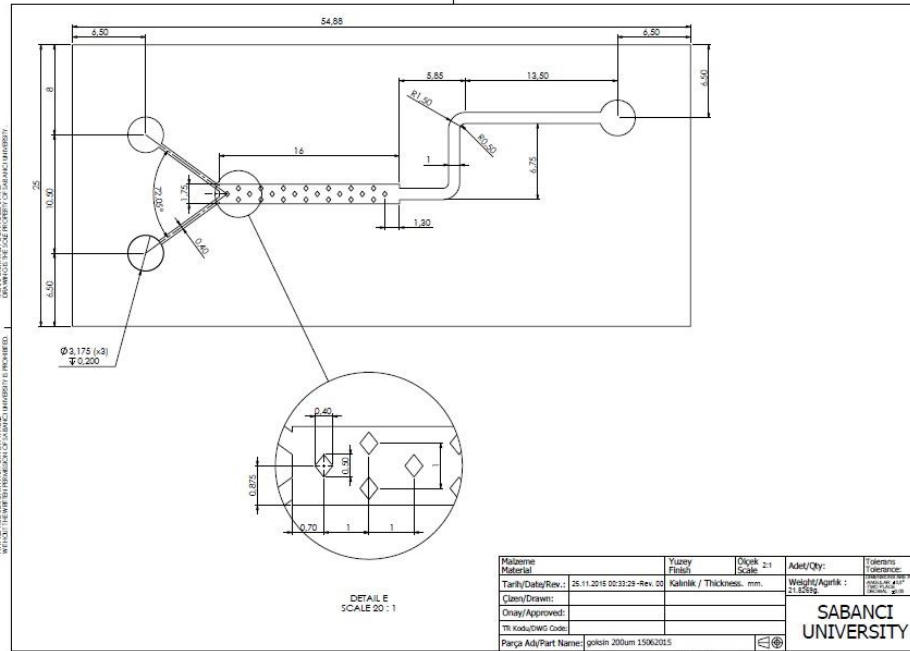


**Figure 13: Adjusted dimensions of microfluidic devices for PDMS fabrication.**

## 2.2.2. Methods

### 2.2.2.1. Experimental Set Up

The general flow of the process was explained in the diagram below. Experimental set up was designed with inlets, transferring tools, micro channels and micro mixing compartment and outlet.

Inputs were given to the system by using a syringe pump. The solutions were loaded into 10 ml sterile syringes, which were placed on the programmable syringe pump. In order to transfer the reactants from the syringe to the microfluidic chip, proper size of tubing was used depending on the dimensions of the microchip. To avoid leakage from the entrance of the micro channels, suitable size of fittings were used in inlets of the microchannels.

The microfluidic chip was designed to be able to have an efficient and quick mixing, after the solutions meet. The chip consists of two inlets, a mixing chamber, a

detection cell, which contains the mixing chamber and micro channel that elongates until the end of the channel, and one outlet. Transparent materials were used for the fabrication of the microfluidic chip, to be able to monitor the mixing and the reaction properly.

The solutions mixed in the chamber were discharged from the outlet of the chip by using tubing and a proper fitting.

The entire process was recorded with a high resolution microscopic camera to be able to record mixing and reaction data. Therefore, the camera was set to be focused on the mixing chamber.

Eventually, the system was washed with distilled water to clean micro channels.

#### **2.2.2.2. PMMA Microfabrication**

The channels were processed on the PMMA chip by CNC micro-machining. Three different sizes of needles were used in different radius and depth. 0.2 mm radius needle was used to process entrance and exit microchannels, whereas, 0.3 mm was used to process inlets and outlets. 0.1 mm radius needles were used to process the area in between the fins in the mixing chamber.

Polyolefin sealing foil is used to bond microchannels. In order to avoid leakage, sealed microchip was compressed in between 2 layers of 3mm PMMA. Compression was supported by screws surrounding the channel. Maximum compression averted leakage. Top layer of PMMA was drilled in the size of fittings.

#### **2.2.2.3. PDMS Microfabrication**

##### **2.2.2.3.1. Acetate mask design and fabrication**

Acetate mask design was a 2D drawing of the micro channels that were to be used as a mask for SU-8. The ability of UV light exposure to harden the material was used to create the channels. Therefore, the channels were designed to be transparent for light to pass through; in contrast, the convex regions were left in black to prevent the light from

penetrating. With the design shown in figure 14, negative master of microfluidic design was obtained.

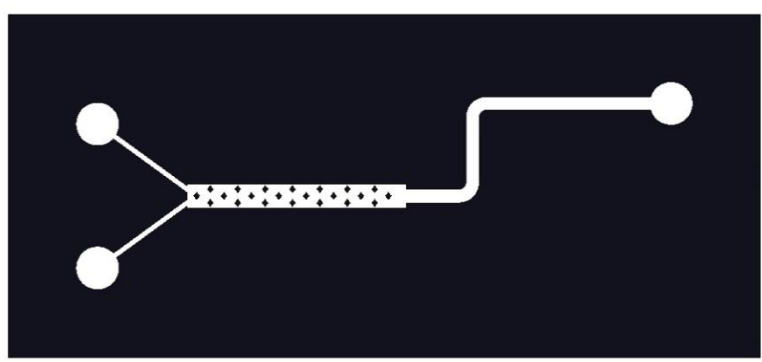


**Figure 14: Photomask design to print on to transparency with high resolution.**

The design was drawn in AutoCad and printed on 10000 dpi printer on A4 size acetate paper.

#### **2.2.2.3.2. SU-8 Photoresist**

SU-8 is an epoxy-based photoresist polymer, which is sensitive to light. SU-8 absorbs in the UV region, because of this reason the light less than 400 nm wavelength initiates molecular binding of SU-8 particles, and causes the material to become rigid. This polymerization process is temperature dependent. SU-8 developer is used to wash the parts that are not exposed to UV light and remains fluidic. SU-8 used in the microfluidic chip fabrication process was ordered from MicroChem. The procedure suggested by the company was followed. The transparency photo mask was designed to have concave regions to be translucent, whereas convex regions to prevent light passage. Because hardening could not be provided in the black regions, those regions were washed out to get rid of the liquid SU-8.

### 2.2.2.3.3. Photoresist Coating of Si-Wafer

SU-8 was used to cover silicon wafer as a photoresist material. The wafer was cleaned with nitrogen gas to get rid of the dust. Because the viscosity of the photoresist material is high, the covering process was performed on the spinner. The wafer was located at the center of the spinner and vacuumed to achieve stabilization. Locating the wafer at the center was a crucial step to have a uniform propagation of SU-8. After placement, approximately 3 ml of SU-8 was poured in the middle of the silicon wafer. For the propagation of SU-8, the wafer was spun at 500 rpm for 10 seconds followed by 1800 rpm spinning for 30 seconds. 80-90  $\mu\text{m}$  thickness was targeted (Figure 15). Because this design is on the microscale, it is accepted to be a very particle sensitive process. Therefore, the fabrication process took place in the clean room.

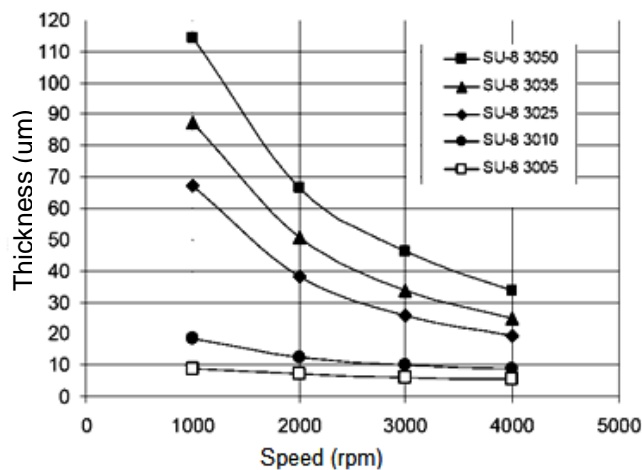


**Figure 15: The speed of the rotation and spinning time was determined by MicroChem Company.**

To provide good attachment between the wafer and SU-8, the wafer was baked on the hot plate at 95°C for 25 minutes, following the spinning. The soft bake duration varying on the thickness was acquired from the SU-8 data sheet.

**Table 2: All the process details are given by the MicroChem Company depending on the thickness.**

Thickness ( $\mu\text{m}$ )	Soft Bake Time (min)	Exposure Energy ( $\text{MJ}/\text{cm}^2$ )	PEB Time ( $65^\circ\text{C}$ ) (min)	PEB Time ( $95^\circ\text{C}$ ) (min)	Development Time (min)
4-10	2-3	100-200	1	1-2	1-3
8-15	5-10	125-200	1	2-4	4-6
20-50	10-15	150-250	1	3-5	5-8
30-80	10-30	150-250	1	3-5	6-12
40-100	15-45	150-250	1	3-5	7-15

#### **2.2.2.3.4. Soft Lithography**

After soft baking process, the SU-8 coated Si-wafer was placed in the lithography machine to be exposed to UV light. The previously prepared acetate mask was placed on the mask aligner. The wafer was exposed to UV light for 14 seconds. The energy provided in 14 seconds was  $250 \text{ MJ}/\text{cm}^2$  (Table 2). After UV exposure, the mask was removed from the wafer and the wafer was subjected to two steps of heating process as post exposure baking (PEB).

PEB process was performed by baking the wafer first at  $65^\circ\text{C}$  for 1 minute, then at  $95^\circ\text{C}$  for 5 minutes on the hot plate. The durations were determined by MicroChem as provided in the Table 2. This process allows the part, which were not exposed to UV light to dissolve.

After PEB, the wafer was left in the SU-8 developer and vibrated on the ultrasonic vibration plate for 15 minute (Table 2.) SU-8 developer allowed the non-solidified material to be cleaned from the wafer. The wafer was washed with distilled water and isopropanol, and then dried with nitrogen gas.

After the wafer was rinsed and dried, it is baked at 150°C for 2 hours. This step is called hard baking. The last baking step provided a chemically and physically stable material to be used as a master for the desired microfluidic chip.

#### **2.2.2.3.5. Characterization of SU-8 master**

The SU-8 master was examined under the microscope to see if there were errors in the channels. The depth of the channels was measured by Profilometer.

#### **2.2.2.3.6. PDMS casting of the SU-8 master**

For PDMS casting, a petri dish plate was prepared by coating with aluminum foil. The SU-8 master was placed on the plate by sticking on the foil. Double sided tapes were used to avoid leakage. PDMS solution was prepared by mixing liquid PDMS with 1:10 of PDMS curing agent. The mixture was whipped well. A homogenous solution was poured on top of the SU-8 master in the petri dish by avoiding bubble production. The air bubbles were removed by placing the petri dish in the degassing oven for 45 minutes. Afterwards, the PDMS was heated in the oven at 75°C overnight (12 hours).

Solid PDMS was gently removed from SU-8 master mold by using a scalpel. The channel profile was cut in the proper size. The master is reusable unless it gets damaged. Therefore, it was preserved in a petri dish covered with aluminum foil to avoid light. The inlets and outlet of the micro channel was drilled with a puncher.

#### **2.2.2.3.7. O<sub>2</sub> plasma bonding**

The PDMS micro channels were bonded to glass micro slides. Both the micro slides and PDMS microchip were rinsed with isopropyl alcohol and distilled water, and then dried with nitrogen gas. After cleaning, the PDMS channel was located in the plasma device, the

channels facing up. The device was vacuumed for 10 seconds, and the channels were exposed to O<sub>2</sub> plasma for 60 seconds.

Finally, PDMS micro channels were pasted on the glass micro slide and left on the hot plate at 75°C for 15 minutes.

#### **2.2.2.4. Mixing Analysis Method**

The evaluation of mixing mechanism of the system was performed by monitoring fast and color changing reactions using a pH indicator called bromocresol green. The chemical properties of bromocresol green allow it to remain green between pH values of 3.8 – 5.4. When the pH value is lowered down to 3.8, the color turns into yellow whereas, when the pH is increased over 5.4, it turns into blue. In this study,  $7 \times 10^{-4}$  M of bromocresol green solution and  $4 \times 10^{-3}$  M of acetic acid is used to test mixing efficiency. The  $k_d$  value of this reaction is indicated as  $5 \times 10^{10} \text{ M}^{-1} \text{ sec}^{-1}$  in the literature [30].

We assumed that bromocresol green and acetic acid reacts faster than the mass transfer in the mixing chamber. Thus, the color change was directly used to probe the mass transfer kinetics of the flows. Reaction time was neglected. The mixing time was accepted as the dead time for this design. Later, for the following protein systems, we assumed that the protein- ligand interaction is slower than the mass transfer, and in this case color change will reflect the iron binding to protein (Figure 16). The mixing time of the chamber could be evaluated and optimized by following the color change.



**Figure 16: At constant flow rate, the distance of the fluid traveled is proportional to time.**

The mixing time was calculated by the ratio of volume of fluid travels per mm to flow rate. The volume of the mixing chamber was accepted as 0.2 ml and the pin-fin volumes in the chamber were neglected. The relationship between mixing time and distance is optimized for different flow rates.

## 2.3. RESULTS

### 2.3.1. PMMA

PMMA design was tested in different volumetric flow rates,  $Q$ . The device was calibrated for each flow rate as shown in Figure 17. Same volumetric amount of acetic acid and bromocresol green was pumped to the mixing chamber by syringe pump and the distance of the complete mixing was measured.

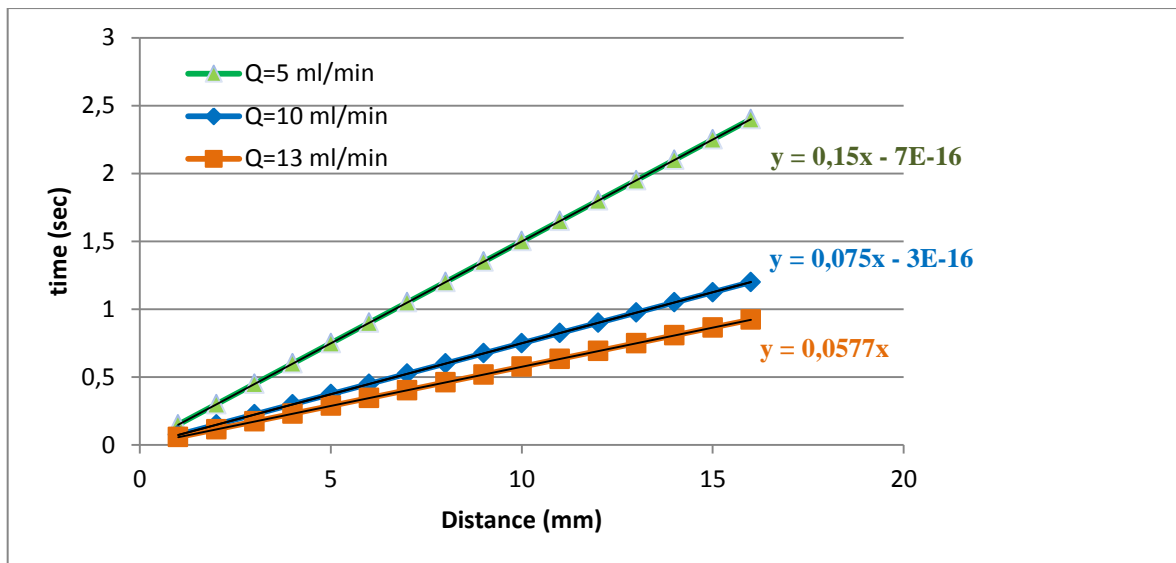


Figure 17: The time is calculated by calibration of the mixing chamber by distance and flow rate.

The microfluidic chip was monitored at the flow rate of 5 ml/min, 10 ml/min and 13 ml/min. Figure 18 shows the flow at  $Q=5$  ml/min. At this flow rate no mixing in the mixing chamber was observed. The only mixing of two reactants was monitored at the interface.

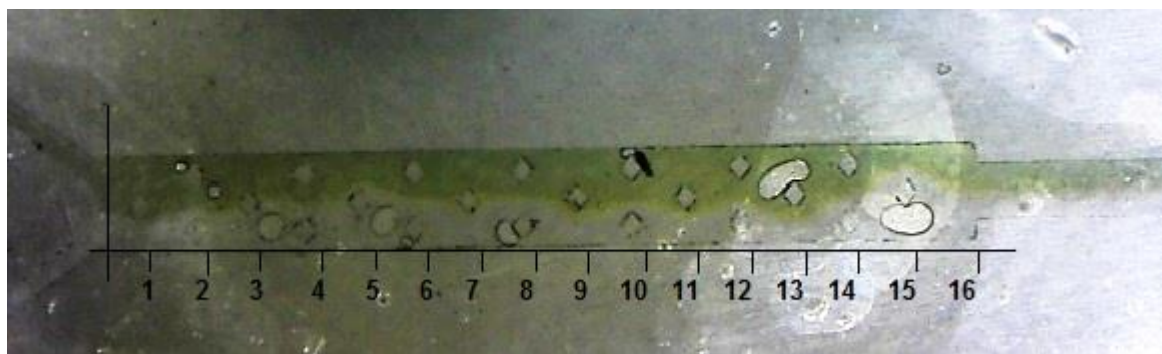
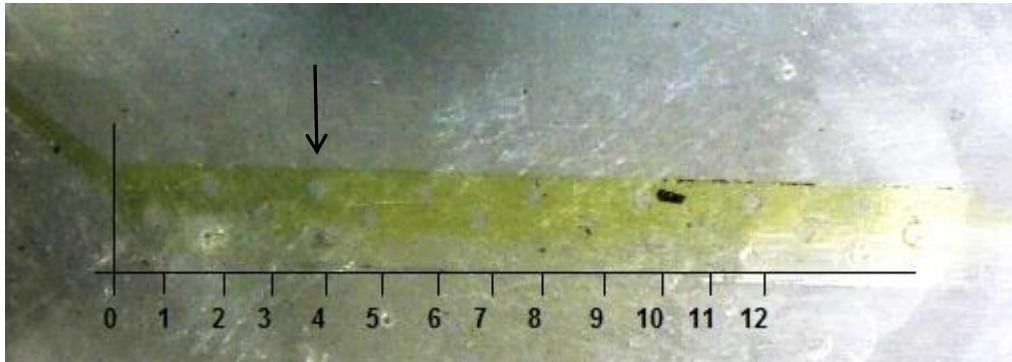
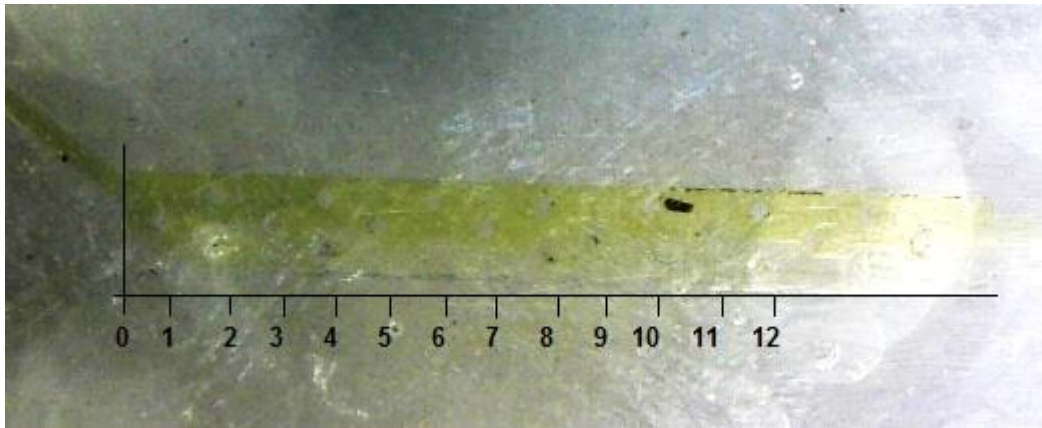


Figure 18: The flow was recorded at  $Q = 5$  ml/min.

When the flow rate was increased to 10 ml/min, the fluid inside the mixing chamber turned into yellow at 4 mm distance (Figure 19). Therefore, after 4 mm, the fluids were completely mixed. The mixing time was calculated as 0.3 seconds by using the equation in Figure 17.



**Figure 19: The flow was recorded at  $Q = 10$  ml/min.**



**Figure 20: The flow was recorded at  $Q = 13$  ml/min.**

The system's limitations were also tested by increasing the flow rate. The maximum flow rate that the microchannels were endured was 13 ml/min (Figure 20). The mixing was observed at 3 mm. Therefore the mixing time was calculated as 0.225 seconds.

### 2.3.2. PDMS

The PDMS microfluidic chip was tested. The mixing chamber was calibrated according to the volume of the design and flow rate. The fabrication of the PDMS chip was performed by lithography and the depth was reached to 87  $\mu\text{m}$ . Accordingly, the dimensions of the mixing chamber was accepted as 1.75 x 16 x 0.087 mm. Since, the volume of the pin-fins are negligible, total volume of the mixing chamber was accepted as  $2.4 \times 10^{-3}$  ml. The time was calculated as a function of distance and flow rate shown in the Figure 21.

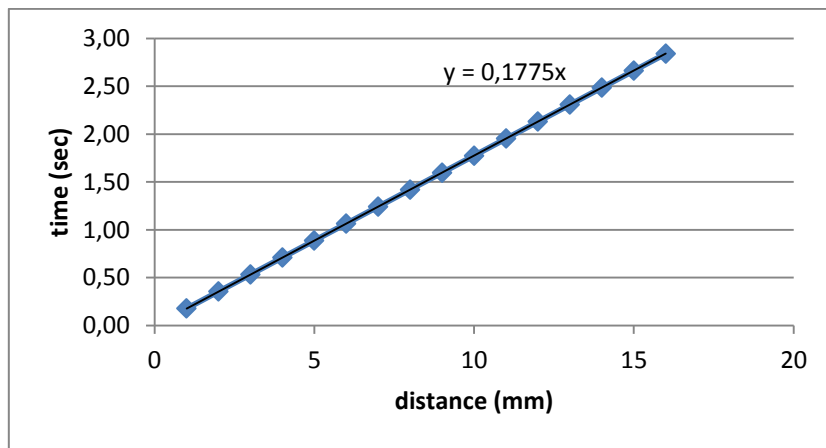


**Figure 21: Time was calculated as a function of distance.**

The limitations of the PDMS design were higher than PMMA design. First of all, because of the lower Young's module value of the material, the channels were resistant to high flow rates. The tests were completed at flow rate values between 500  $\mu\text{l}/\text{min}$  and 2 mg/ml (Figure 22).

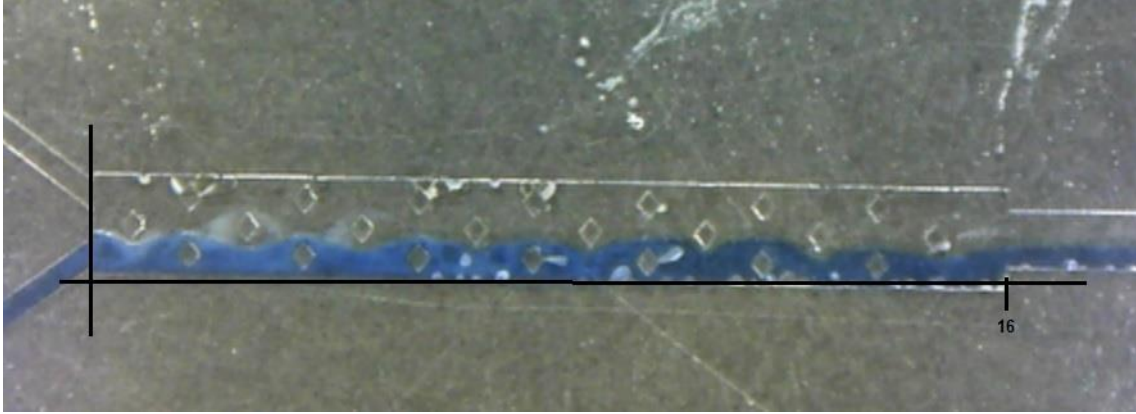


**Figure 22: The flow caption at  $Q=500 \mu\text{l}/\text{min}$  in PDMS design.**

### **2.3.3. Simulations**

The experimental results were not found convincing. Because of time and cost limitations, numerical simulations were run in order to optimize the micromixing channel of the design. Commercial tool based on finite volume, ANSYS Fluent 14.0 was used to numerically investigate the hydrodynamic characteristics of mixing flow in a pin finned micro channel. To set up the system, the Volume of Fluid (VOF) model is utilized to solve the equations of mass and momentum conservation, which enabled modeling of multiple separate, yet interacting phases.

The computational domain comprised of a micro channel with a width of 2.5 mm and length of 16 mm, where diamond-shaped pin-fins decussate inside the channel with a length of  $500 \mu\text{m}$ , as shown in Figure 23. With a total element number of 40000, FVM was used to discretize the governing equations as described above. For pressure-velocity coupling and the approximation of convection terms, coupled algorithm and second order schemes were used, respectively. For both phases, uniform inlet mass velocity was considered as the boundary condition of the hydrodynamic inlet. Physical properties of the fluid concerned were kept constant and atmospheric pressure was ensured at the outlet. No-slip condition was enforced for the velocity at wall boundaries. Physical properties of fluids concerned are shown in Table 3. The viscosity of bromocresol green was accepted the same

as viscosity of water, since the solution was prepared in distilled water. It was noted that both fluids enter the channel with flow rate of 5 ml/min.

**Table 3: Physical properties of bromocresol green and acetic acid at room temperature**

Characteristics	Bromocresol Green	Acetic Acid
Viscosity	0.9 mPa.s	1.131 mPa.s
Density	0.79 g/ml	1.05 g/ml

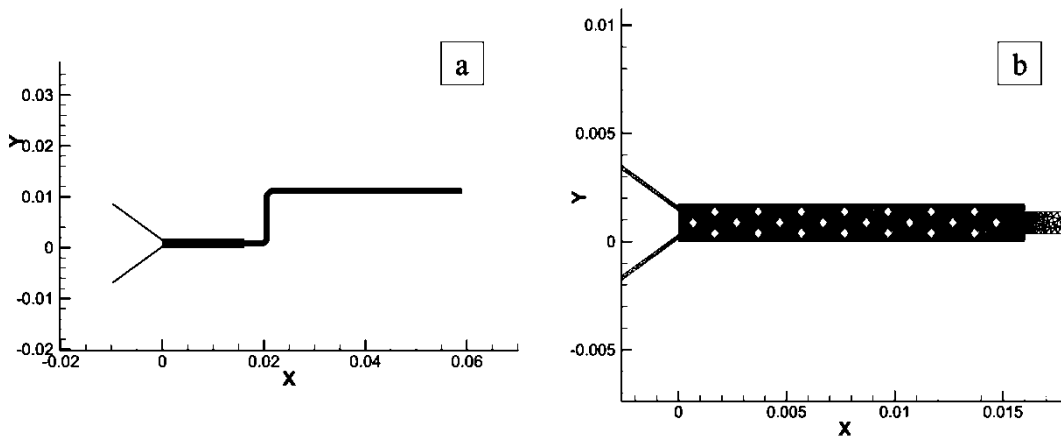


**Figure 23: The schematic computational domain identified to program: (a) shows the microchannels in microfluidic chip, (b) shows only the mixing chamber.**

The ANSYS Fluent results for the designs were supportive with the experimental results. The pin-fin conformation was not as effective as predicted (Figure 24). In order to get a good mixing, the flow rate has to be increased to a value where the consumption of

sample volume is intolerable. Hence, other channel geometries were also analyzed for optimization.

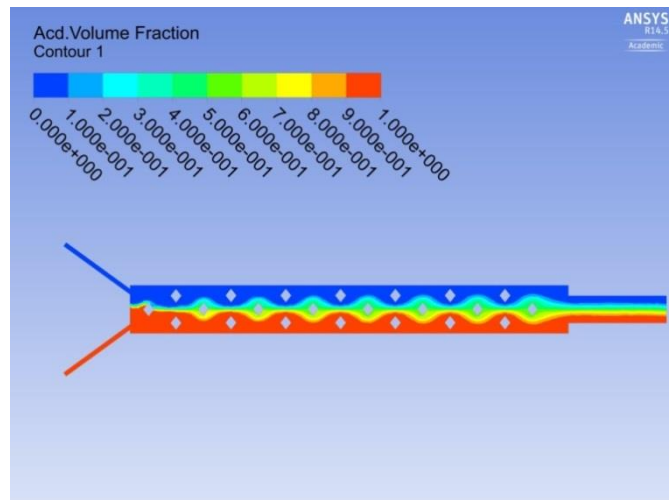


**Figure 24: Numerical analysis of micromixing channel geometry with pin-fins at flow rate  $Q=10$  ml/min.**

### **2.3.3.1. Effect of channel size on mixing effect**

Effect of channel size on mixing is shown in Figure 25. Mixing was more pronounced in a smaller channel, mainly due to higher velocity of fluids in the channel.

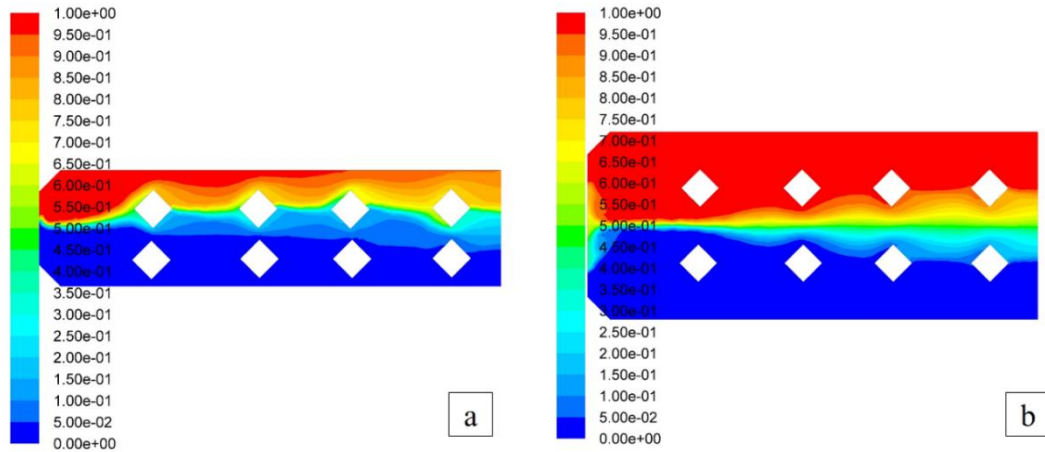


**Figure 25: Effect of channel size on mixing phenomena.** The scale on the right represents the channel size. (a) displays a channel with a width of 2 mm whereas, (b) displays a channel double the size of a.

### 2.3.3.2. Effect of pin fin distribution on mixing

Pin-fin distribution had negligible effect on mixing phenomena. Comparing obtained results of Figure 25 and Figure 26, it can be concluded that the channel size was much more effective in mixing than the shape of the fins.

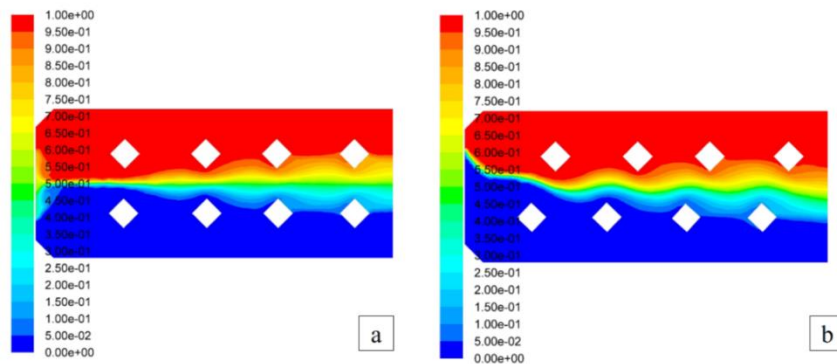


**Figure 26: Effect of pin-fin distribution on mixing.**

### 2.3.3.3. Future potential design

The numerical analysis suggested that pin-fin conformation and the width of the channels were primary effects on the micromixing in the lower flow rates. Creating a

higher surface area for the fluids to meet is essential for a successful design. Creating a strait on the pathway would provide the highest mixing efficiency at lower flow rates, meaning lower sample consumption. Figure 27 is the numerical representation of such a design, where the flow rate is between 0.1 – 1 ml/min. This region is compatible with other microfluidic devices.

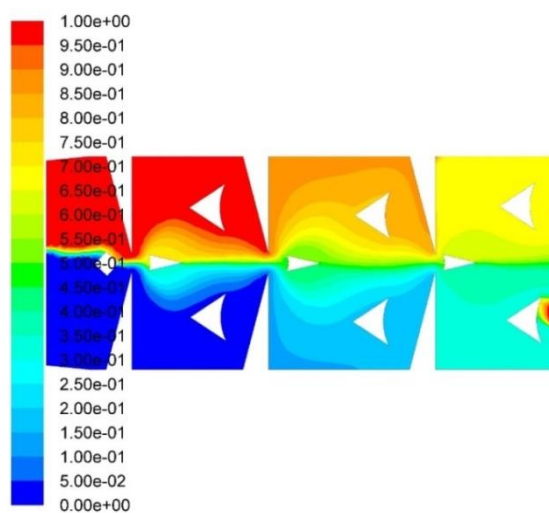


**Figure 27: Potential future design at  $Q=0.3$  ml/min**

## **CHAPTER III – EXPRESSION AND PURIFICATION OF *HAEMOPHILUS INFLUENZAE* FERRIC BINDING PROTEIN IN APO-FORM**

### **3.1. BACKGROUND**

The importance of iron for both human and bacteria is explained in details in Chapter I. The specific mechanism developed by bacteria to hijack iron from host organisms is emphasized in recent studies. In most cases, proteins are commercially available for researchers. However, because proteins vary depending on the originated organism, rare proteins are needed to be synthesized in vitro. Advanced molecular techniques are found beneficial to such studies. Genetic modification of the organisms expedites research studies on these subjects.

In this study, *Haemophilus Influenzae* Ferric Binding Protein has been expressed and characterized in the laboratory. The characteristics of iron uptake mechanism by the bacterial FBP remain the same in the protein obtained by recombination techniques in vitro. Since the study on *Haemophilus Influenzae* as a pathogenic Gram – Negative bacteria is threatening and risky process, most of the applications on this topic is performed by using another Gram – Negative bacteria, *Escherichia coli*.

Recombination technology is a promising engineering study that eliminates many limitations in the laboratories [31]. With this technology, it is possible to construct the DNA of *E. coli* by transforming a circular piece of DNA fragment. It is a very popular technique in protein engineering. The practice of recombination techniques in this study can be explained as; the insertion of a particular engineered DNA sequence into a circular piece of DNA from specific sites [32]. This specific sites are called restriction sites, which are digested by site specific enzymes, restriction enzymes. Restriction enzymes are nucleases which recognize specific DNA sequence to bind and cleave from that location [33]. In the construction of a DNA segment, restriction sites matching with multiple cloning site of the plasmid is synthetically built. Therefore, cleaved DNA fragment can be placed with the particular DNA sequence. Once it is inserted into the plasmid, plasmid is

transferred into *E. coli* and multiplied there. That allows the augmentation of the desired DNA sequence [34].

Cloning vectors are piece of circular DNA containing an antibiotic resistance gene, promoter, multiple cloning site and ribosomal binding site. When the vector is transformed into bacteria, the antibiotic resistance gene allows it to survive in presence of that specific antibiotic [35]. This characteristic is profitable for eliminating non-desired organisms in the working medium. On the other hand, multiple cloning sites accommodate several restriction sites. Thus, they are serving as an insertion site for synthetic DNA fragments in recombination technology. Furthermore, promoter and ribosomal binding site are responsible of expression. All these compartments are required in a cloning vector for molecular techniques.

Metal affinity separation is an acknowledged method in protein expression. Presence of multiple histidine residues in the amino acid sequence makes it easier to separate, because of the high affinity of histidine residues to metals [36]. Thus, when the DNA fragment is designed, six histidine residues are put at the beginning of the desired amino acid sequence or the DNA fragment is inverted into a vector that contains these residues. After the protein synthesized, his-tag can be cleaved. Another charming method is being used to remove histidine tag from the genetically engineered fusion protein. TEV cleavage site is a specific amino acid sequence, discovered from tobacco etch virus [37]. This site is recognized by a protease enzyme and cut. Therefore, its specific sequence is inserted in between desired amino acid coding sequence and histidine tag, in order to obtain the protein by itself.

Previously mentioned molecular techniques formed our path to express *Haemophilus Influenzae* FBP in laboratory conditions.

## **3.2. MATERIALS AND METHODS**

### **3.2.1. Materials**

#### **3.2.1.1. Chemicals**

Chemicals used in the study are listed in Appendix A.

#### **3.2.1.2. Equipment**

Equipment used in the study are listed in the Appendix B.

#### **3.2.1.3. Software and Programs**

CLC Main Workbench 7

### **3.2.2. Methods**

#### **3.2.2.1. Preparation of LB Growth Media**

In order to prepare liquid media, 10 g of Tryptone, 5 g of NaCl and 5 g of yeast extract was dissolved in 1 L of distilled water and autoclaved at 121°C. For the selective medium, the final concentration of 50 µg/ml kanamycin (KAN) was added and stirred.

For the solid LB medium, 15 g of Agar was dissolved in 1 L of liquid LB medium. For selective medium, the final concentration of 50 µg/ml KAN was added and stirred. The liquid medium was immediately poured into sterile plates and autoclaved at 121°C.

#### **3.2.2.2. Preparation Buffers and Solutions**

All the buffers and solutions were prepared based on the equation 6 and equation 7.

$$\text{molarity} = \frac{\text{mass}}{\text{Molecular weight} \times \text{volume}} \quad (6)$$

$$M = \frac{m}{MW \times V}$$

$$\text{Initial Concentration} \times \text{Initial Volme} = \text{Final Concentration} \times \text{final Volme}$$

$$C_1 \times V_1 = C_2 \times V_2 \quad (7)$$

The following steps were completed accordingly.

- A. CaCl<sub>2</sub> solution 1: 80 mM CaCl<sub>2</sub> and 50 mM MgCl<sub>2</sub> was dissolved in 500 ml of distilled water and autoclaved at 121°C.
- B. CaCl<sub>2</sub> solution 2: 0.1 M CaCl<sub>2</sub> was dissolved in 500 ml of distilled water and autoclaved at 121°C.
- C. TAE (Tris-Acetate-EDTA) buffer: For 50X stock solution; 242 g Tris base was dissolved in 100 ml 0.5M sodium EDTA. 57.1 ml 100% acetic acid was added. Distilled water was added up to 1L. The stock solution was diluted to 1M for gel electrophoresis.
- D. HEPES buffer: 500 ml of HEPES buffer at pH 7.5 was prepared for the BugBuster protocol. 200 mM NaCl and 20 mM HEPES was dissolved in 500 ml of distilled water. pH was adjusted to 7.5 by adding NaOH.
- E. Purification buffer: 100 ml of 10X purification buffer was prepared for the purification of the proteins. 500 mM Tris.HCl, 3M NaCl, 200 mM imidazole, 50 mM MgCl<sub>2</sub>, 300 μM Al<sub>2</sub>(SO<sub>4</sub>)<sub>3</sub> and 100 mM NaF was filled with 100 ml distilled water. pH was adjusted to 8 by adding NaOH.
- F. Washing buffer: 150 ml of washing buffer was prepared to be used in the protein purification protocol. 1X purification buffer, 10 mM BME and 0.2 mM PMSF was mixed and filled up to 150 ml with distilled water.
- G. Elusion buffer: 50 ml of elusion buffer was prepared by adding 280 mM imidazole into 50 ml of washing buffer.
- H. Dialysis Buffer: 4 L of dialysis buffer was prepared to be used to remove imidazole after purification. 50 mM Tris.HCl, 100 mM NaCl and 1 mM EDTA was filled up to 4 L of distilled water. The pH of the solution was adjusted to 8 by adding HCl.
- I. Sodium citrate washing buffer: 100 ml of washing buffer was prepared to be used in the process of removing iron from FBP. 1 mM EDTA and 4000-fold

Sodium Citrate was dissolved in the 100 ml of distilled water. pH of the solution was adjusted to 7.5.

- J. PO<sub>4</sub> solution: 10 ml PO<sub>4</sub> solution was prepared by dissolving 5 mM Na<sub>2</sub>HPO<sub>4</sub> in distilled water to be used in the process of removing iron from FBP.
- K. Exchange buffer: 100 ml of exchange buffer was prepared to change the EDTA buffer to Tris buffer after removing the iron from the protein. 10 mM Tris was dissolved in the 100 ml distilled water. pH was adjusted to 8 by adding HCl.

### **3.2.2.3. Construction of pET-28a (+) containing Ferric Binding Protein encoding gene**

The sequence of the gene, expressing Ferric Binding Protein (FBP) in *Haemophilus Influenza*, was taken from the NCBI. The exact DNA sequence was optimized for expressing the protein in *Escherichia coli* by the Genscript Company. Optimized sequence was cloned into commonly used vector called pET-28a (+) with some additional sites in order to make the protein easy to purify. One of these sites was called His-Tag that exists in the vector. For the ease of purification step, a nucleotide sequence encoding a bunch of histidine residues were added to the vector after the first restriction site. In this protein five histidine residues were added as CAT codons. His-Tag site has high affinity to the metal chelates such as Cu<sup>+2</sup>, Ni<sup>+2</sup>, Zn<sup>+2</sup>, Co<sup>+2</sup>. Having a histidine tag concedes the desired protein to be separated by using a metal chelate affinity column up to 95% purity [38]. Another site which was inserted to the original sequence was tobacco etch virus (TEV) protease cleavage site. This site is usually added to the N- terminal of the protein, following the histidine tags as a very selective amino acid sequence [39]. This specific sequence was given in the literature as ENLYFQ followed by S or G at the end, where the cut has been done after Q in optimum conditions [40]. The nucleotide sequence encoding the given amino acid sequence, which is known to be very selective to the TEV protease enzyme, was inserted to the beginning of the FBP encoding sequence, just after the string that encoded five histidine residues. GAAAACCTGTATTTTCAGAGC was the optimized nucleotide sequence determined by the Genscript Company. Finally a stop codon was added to the end of the sequence encoding FBP. The engineered gene, accommodating His-

Tag, TEV site and stop codon at the end, was cloned into pET-28a(+) by NdeI and XhoI. Therefore, they were located between NdeI and XhoI restrictions sites of the vector.

The plasmid was received in solid state as 4 µg. The vial containing the plasmid was first centrifuged at 6000 x g for 1 minute at 4°C. 10 µl of sterilized water added and the vial was shaken on vortex machine to dissolve the sample. A concentration of 0.4 µg/µl was obtained at the end. The gene was multiplied by expressing in the *E. coli* by following the steps below;

#### **3.2.2.4. Preparation of component cells:**

TOP10 and BL21, which are two different genotypes of *E. coli*, were used in this study for expressing FBP. Solid and liquid cultures containing these types of bacteria were prepared.

BL21 and TOP10 stocks, which were kept in the -80°C freezer, were streaked on the non-selective LB plates and incubated at 37°C overnight (12-16 hours). The growth of bacterial colonies was observed on the solid medium.

To prepare the small liquid culture, one colony was picked from each TOP10 and BL21 plates, inoculated into 5 ml of liquid LB without kanamycin. The cultures were incubated at 37 °C under shaking at 270 rpm overnight. The growth of bacteria caused turbidity in the liquid LB medium.

To prepared the big liquid culture, 2 ml of starter culture from each types of *E. coli* was added to 200 ml liquid LB medium and left to grow in 37°C shaking incubator. The OD<sub>600</sub> was measured until it reached 0.94. In most cases, OD<sub>600</sub> value of 0.94-0.95 was determined as the most effective value to obtain the highest amount of potential competent cells in the *E. coli* growth cycle [41]. Since the population growth of the bacteria increases exponentially, the OD<sub>600</sub> values were measured every half an hour at the beginning. After 2 hours the values were measured more frequently. When OD<sub>600</sub> value had reached 0.94, cultures were put on ice and left for cooling. Therefore, the growth of the populations was decelerated and paused.

After 20 minutes of incubation on ice, the competent cells were extracted for storage. 200 ml cultures of BL21 and TOP10 was transferred into previously cooled centrifuge bottles. The cells were harvested at 3000 x g (~4000rpm in the Beckman JA-10 rotor) for 15 minutes at 4°C. The supernatant were decanted, whereas the pellet was resuspended mildly in 4 ml of cold CaCl<sub>2</sub> solution 1. The vials were kept on ice for 10 minutes. Similar to the previous step, the cells were harvested by centrifuging at 2000 x g (~3000 rpm in the Beckman JA-10 rotor) for 15 minutes at 4°C. The supernatant was discarded and the pellet was resuspended again in the CaCl<sub>2</sub> solution 1. The cells were harvested one more time at 2000xg (~3000 rpm in the Beckman JA-10 rotor) for 15 minutes at 4 °C. The supernatant was decanted, and the pellet was resuspended in 1 ml of cold CaCl<sub>2</sub> solution 2. 15% of glycerol was then added. Aliquot of 90 µl was put into previously cooled 1.5 ml microfuge tubes and snapped frozen with liquid nitrogen. The final frozen cells were stored in the -80°C freezer to be used as necessary.

#### **3.2.2.5. Transformation of the engineered pET-28a (+) into TOP10 and BL21:**

The recombinant pET-28a(+) plasmid with the FBP gene, ordered from Genscript Company, was transferred into both TOP10 and BL21 for multiplication and expression of the protein by following the procedure in “Molecular Cloning: A laboratory manual” by Sambrook et al., 2001.

Transformation was done in both types of *E. coli* cells, whereas, the expression was only performed in BL21. The construct was transformed into TOP10 for the purpose of multiplication. Therefore, more plasmids were obtained and transformed into BL21 for more expression of the FBP protein.

Transformed *E. coli* cells were strained on the LB plates. Kanamycin was used as a selective antibiotic for the construct cells. The plates were located inverted in the 37°C incubator overnight.

Small liquid culture was grown in the presence of kanamycin.

### 3.2.2.6. Isolation of plasmid DNA

Plasmid isolation was performed by following the Qiaprep Spin Miniprep Kit procedure. By following this procedure, the bacterial cell membrane was lysed under alkaline conditions. Bacterial chromosomes sticking to the membrane was removed and plasmids that are free in the cytoplasm were obtained. The plasmids were kept on silica filter in the presence of high salt concentration, whereas bacterial DNA was eliminated by removing the supernatant. Lastly, the column was eluted with water in order to get plasmids.

The plasmids isolated from TOP10 cells were transformed into BL21 cells for the expression of the protein by following the procedure in part 2.2.2.5., then isolated for confirmation. Concentration of the plasmids was determined by NanoDrop spectrophotometer at 260 nm.

**Table 4: Concentrations of TOP10 and BL21 cells after transformation**

Name	Concentration	Name	Concentration
TOP10 – I	70 ng/μl	BL21 – I	202.5 ng/μl
TOP10 – II	148.9 ng/μl	BL21 – II	169.9 ng/μl

Glycerol stocks were prepared by adding 15% glycerol into the 2 ml tubes and frozen in the liquid nitrogen tank. Later, stocks were placed in the -80°C freezer.

### 3.2.2.7. Digestion of the plasmid with restriction enzymes NdeI and XhoI

Constructed DNA sequence was cut from isolated plasmid by NdeI and XhoI restriction enzymes for confirmation. Double Digestion Calculator provided by Thermo Scientific was used to determine the conditions. 2X Tango Buffer, 2 fold excess NdeI and

XhoI was recommended. 1 µg of TOP10 and 1.5 µg of BL21 plasmids were digested. Tubes were incubated at 37°C for 1 hour.

**Table 5: Digestion of the plasmid from the restriction sites to cut the gene**

	<b>Top 10 – I</b>	<b>Top 10 – II</b>	<b>BL21 – I</b>	<b>BL21 – II</b>
Plasmid	14.3 µl	6.7 µl	7.4 µl	8.8 µl
2X Tango Buffer	6 µl	4 µl	6 µl	6 µl
XhoI	2 µl	2 µl	2 µl	2 µl
NdeI	4 µl	4 µl	4 µl	4 µl
dd-H <sub>2</sub> O	3.7 µl	13.3 µl	10.6 µl	9.2 µl
Final Volume	30 µl	30 µl	30 µl	30 µl

### **3.2.2.8. Confirmation with agarose gel electrophoresis**

Cut DNA was run on the agarose gel for confirmation. The size of the gene was determined.

Agarose gel in concentration of 1 % was prepared. 1 g of agarose was liquefied in 100 ml of 1X TAE buffer by heating for 3 minutes in a microwavable flask. TAE buffer helps the agarose to be polymerized. Then, final concentration of 0.2 µg/ml ethidium bromide was added into the solution. Ethidium bromide binds to DNA and makes it visible

under UV light. The solution was poured into gel tray and suitable sizes of well combs were placed. The gel was left for solidification for 30 minutes at room temperature.

1 % agarose gel was placed in the gel box filled with 1X TAE buffer. Uncut plasmids and cut DNA were sampled. Samples were mixed with 6X loading dye and loaded into the wells. Molecular weight marker was loaded as a reference. The samples were run on the gel at 110 Volts for 40 minutes.

### **3.2.2.9. Expression of FBP in BL21 cells**

The expression of the ferric binding protein was only performed in BL21 cells, because of their high efficiency of expressing proteins. Before starting, the small culture containing constructed BL21 cells was carried out and left for growing overnight at 37°C under shaking.

2 ml of starter culture was added to 200 ml of liquid LB medium in the presence of kanamycin. Cells were grown in the 37°C incubator under shaking until the OD<sub>600</sub> value was measured as 0.6.

The cells were induced by decreasing the temperature of the incubator down to 26°C and adding final concentration of 0.7 mM IPTG (isopropyl-beta-D-thiogalactopyranoside). After 5 hours of incubation, cells were transferred into centrifugation tubes and centrifuged at 7000 rpm for 30 minutes at 4°C. Supernatant was discarded whereas the pellet was kept in the -80°C freezer.

### **3.2.2.10. Purification of Ferric Binding Protein**

All buffers were prepared as mentioned in section 2.2.2.2. and kept in 4°C.

#### **3.2.2.10.1. Lysis of the cells by BugBuster protocol**

The cells were lysed in order to get the expressed protein out of the cell by following the BugBuster protocol by NOVAGEN. The pellets were weighted and resuspended in 5 fold of BugBuster, filled up to 25 ml of HEPES buffer. 1 tablet of EDTA

free protease inhibitor was dissolved in the solution. Resuspension was done by pipetting. 1  $\mu$ l of benzonaze was added per ml of BugBuster for resuspension. Everything was transferred into falcon tubes and left on the shaker for 20 minutes at room temperature. Solution was transferred back to centrifugation flasks and centrifuged at 16000 g for 20 minutes at 4°C. Beckman JA-10 rotor was used. Finally, supernatant was kept in the falcon tube at 4°C.

#### **3.2.2.10.2. Ni-affinity column purification of FBP**

The ability of histidine residues to bind Ni beads allows the protein to be separated. Six histidine residues were constructed into the FBP via the vector containing encoding gene [42]. Columns that contain slurry Ni-NTA agarose were used for purification. All the procedure was performed at 4°C.

Ni columns were equilibrated with purification buffer at the beginning. The FBP containing supernatant obtained after the lysis of the cells were mixed with resin and let shaking in the 4°C cold room to bind Ni. After 1 hour, the flow through was collected.

In the washing step, the columns were washed three times with washing buffer. Each time, they were incubated in the buffer for 5 minutes. Afterwards, the proteins were eluted by adding elusion buffer. The columns were incubated again for 5 minutes. The FBP accommodating flow through was collected. Elution step was repeated three times in order to get highly pure protein. The final protein solution contains imidazole for stabilization.

#### **3.2.2.11. SDS-Page check**

Proteins were analyzed by 12% sodium dodecyl sulfate polyacrylamide gel electrophoresis (SDS-PAGE) [43]. Gels were stained with Coomassie colloidal brilliant blue according to the protocol described by Dyballa and Metzger [44]. The mixture of molecular weight markers were provided by Page Ruler™ unstained protein ladder Thermo Scientific.

### **3.2.2.12. Dialysis of the FBP to remove imidazole**

As a final purification step, dialysis was performed in order to remove the imidazole from the protein sample. Free imidazole causes denaturation of the protein. Therefore, it should have been removed before going into further steps [42].

The dialysis buffer was prepared as it is described in the section 2.2.2.2. 15 ml of protein sample was put into dialysis against 2 L dialysis buffer. The sample was left in 4°C cold room. Dialysis buffer was changed after 6 hours and left in the cold room for another 6 hours. Eventually, FBP bonded to  $\text{Fe}^{+3}$  ions were acquired in dialysis buffer.

### **3.2.2.13. Removing $\text{Fe}^{+3}$ ions from holo-FBP**

To remove the iron from the protein, the suggested protocol in “High resolution structure of an alternate form of the ferric ion binding protein from *Haemophilus Influenzae*” by Stephen R. et al. was followed [45].

15 ml of protein solution was transferred into Centricon 10. The sample was centrifuged until the volume was aggregated to 5 ml. 10 ml of sodium citrate washing buffer (Buffer I in section 2.2.2.2.) was added to the sample. Then, it was centrifuged again until the volume reached 5 ml. This step was repeated six times. The Centricon containing 5 ml of sample was incubated on ice for 20 minutes. The buffer of the sample was exchanged with 10 mM Tris.HCl solution at pH 8 (Exchange buffer in section 2.2.2.2.). In order to change the buffer of the protein, the sample was washed with 10 ml of buffer and centrifuged until 5 ml of the sample was left. This step was repeated five times. 5 mM of  $\text{Na}_2\text{HPO}_4$  solution was added and the sample was incubated on ice for another 20 minutes (Phosphate solution in section 2.2.2.2.). Lastly, the sample was washed with 10 mM Tris.HCl buffer five times. The remaining 5 ml of protein sample was accepted to be iron free. The concentration was measured with NanoDrop by measuring the absorbance at 280 nm.

### 3.2.2.14. Concentration of the apo-FBP

Apo-FBP in micro tubes was transferred into small Centricon YM-3. Centricon tubes were centrifuged until the volume went down to 1000  $\mu$ l. The concentration of the protein was measured at 280 nm.

### 3.2.2.15. Preparation of FeCl<sub>3</sub> solutions

FeCl<sub>3</sub> solutions were prepared at different concentrations to measure the absorption spectra, in order to be able to compare the Fe<sup>+3</sup> effect on the holo-FBP. Considering the fact that FeCl<sub>3</sub> is not soluble between pH 5-8, the solutions were prepared in water instead of dialysis buffer and the pH was measured as 2.5. 150 ml of 5 mM stock solution was prepared to be diluted later.

10 ml of FeCl<sub>3</sub> solutions were prepared by diluting the stock solutions. The volume of the 5mM stock solution used in the dilution was calculated according to the equation 7.

**Table 6: Stock FeCl<sub>3</sub> solution was diluted into various concentrations**

Concentration	Volume of stock FeCl <sub>3</sub>	
0.01 mM	0.02 ml	Filled up to 10 ml with milli-q water.
0.05 mM	0.1 ml	
0.1 mM	0.2 ml	
0.5 mM	1 ml	

### 3.2.2.16. Bradford assays

Protein concentration was determined according to the method of Bradford, using bovine serum albumin as the standard [46].

## 3.3. RESULTS:

### 3.3.1. Construction of pET-28a (+) containing FBP encoding gene

The amino acid sequence of the protein was received from Protein Data Base, (PDB ID: 1D9V) and is as follows:

DITVYNGQHKEAATAVAKAFEQETGIKVTLSNGKSEQLAGQLKEEGDKTPADV  
FYTEQTATFADLSEAGLLAPISEQTIQQTAQKGVPLAPKKDWIALSGRSRVV  
VYDHTKLSEKDMEKSVLDYATPKWKGKIGYVSTSGAFLEQVVALS  
KMKGDKVALNWLKGLKENGKLYAKNSVALQAVENGEVPAALIN  
NYYWYNLAKEKGVENLKSRLYFVRHQDPGALVSYSGAAVLKASK  
NQAEAQKFVDFLASKKGQEALVAARAEYPLRADVVSPFNLEPYEK  
LEAPVVSATTAQDKEHAIKLIEEAGLK

The gene coding Ferric Binding Protein was optimized for *E. coli* and inserted into pET-28a (+), which has a kanamycin resistance region, with additional His-tag and TEV site for cleavage of the his-tag from synthesized protein after purification.

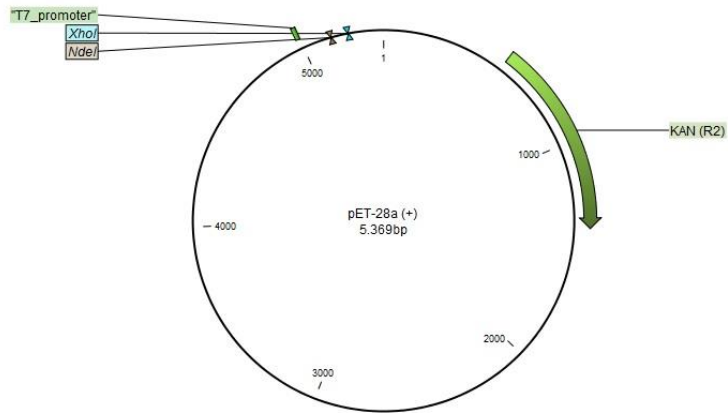


**Figure 28: pET-28a(+) vector with T7 promoter, kanamycin resistance gene, NdeI and XhoI restriction sites**

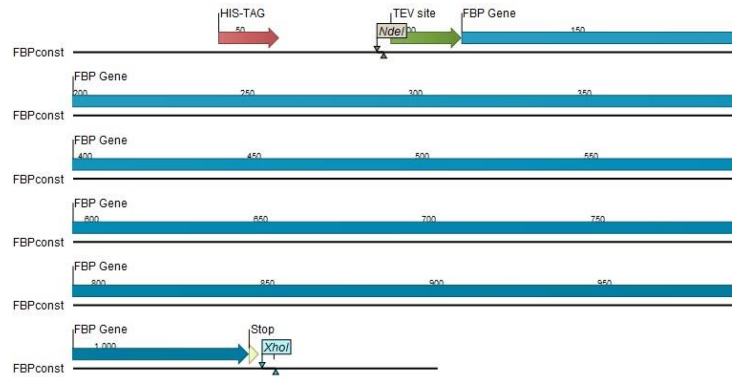


**Figure 29: FBP coding gene sequence with His-tag and TEV site at the beginning and a stop codon at the end.**

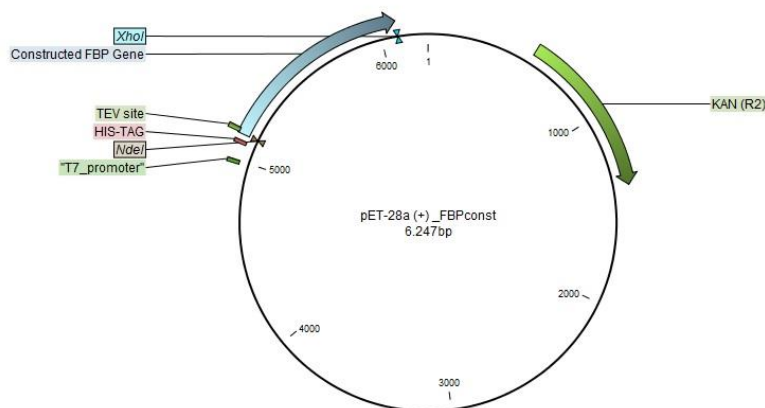


**Figure 30: Constructed FBP coding gene was inserted in between restriction sites NdeI and XhoI.**

### 3.3.2. Transformation of the engineered pET-28a (+) into TOP10 and BL21

pET-28a + FBP construct was transformed into TOP10 and BL21 cells to be multiplied and expressed. The colonies were grown in the presence of kanamycin.

### 3.3.3. Confirmation with agarose gel electrophoresis

After transformation, the plasmid isolated from kanamycin resistant colonies was double digested to confirm presence of the gene by agarose gel electrophoresis. The size of the constructed plasmid and the gene inserted was known from the construction map. We expected to get a band about 7000 base pairs for the plasmid and another band at 990 base pairs.

The construct was transformed into TOP10 cells for multiplication purposes and into BL21 cells for protein expression. Then, plasmids were isolated and FBP coding gene was cut for confirmation. The band at 990 bp confirmed the constructed gene's existence (Figure 31). These results were consistent with the construction map (Figure 31).

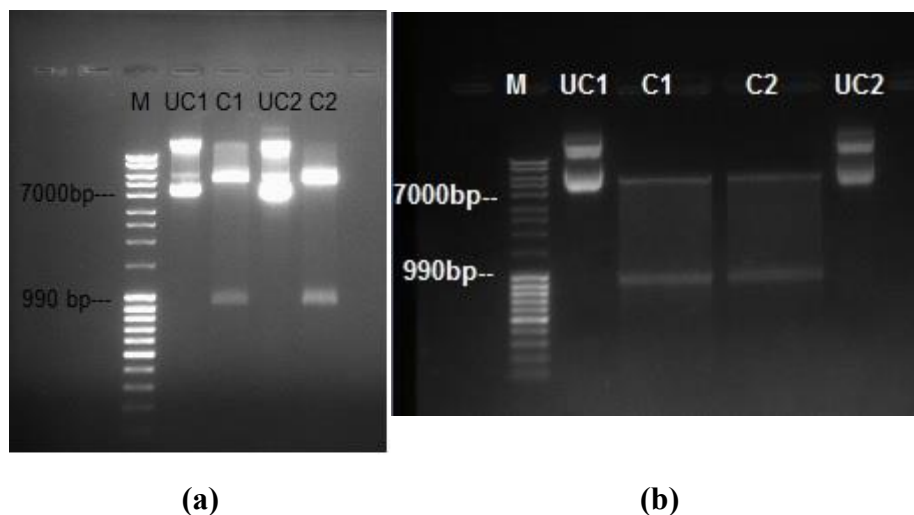


**Figure 31: (a) Agarose gel confirmation of TOP10 cells. (b) Agarose gel confirmation of BL21 cells.**

### **3.3.4. Control of protein expression in E. coli with SDS-page analysis**

The results were analyzed by running SDS – Page, after expression and purification of the recombinant FBP in BL21 cells. In the Ni- affinity purification step, the substantial protein was transferred into the elution solutions, containing imidazole from the column. Therefore, the bands at about 40 kDa appeared on the SDS – gel. These results were promising. Because most of the proteins was attached to Ni – resin in the washing steps, there were not any bands shown for the washing solutions. The presence of bands at 40 kDa proved that we were successfully purified desired protein Figure 32.

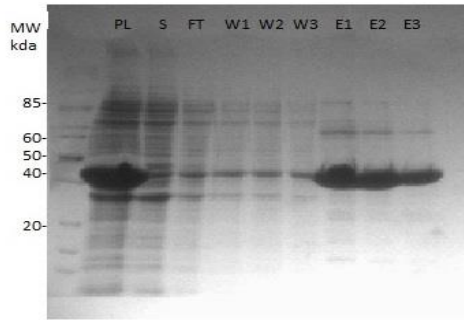


**Figure 32: SDS-Page control of the protein. PL: pellet, S: supernatant, FT: flow through, W: washing, E: elution**

### **3.3.5. Concentration of the protein solution**

To measure the concentration of the protein, dialysis was performed to get rid of imidazole in the protein solution. The reason of removing imidazole before measuring the concentration was because of its interference in absorption. Imidazole gives a peak on the same wavelength as the proteins, which would cause an error on determining the concentration. Thus, protein concentrations were measured after the dialysis with NanoDrop by measuring the absorbance value at the UV-Visible wavelength. The concentration of the holo – protein was measured as 1.047 mg/ml. A peak at around 280 nm was obtained (Figure 33).

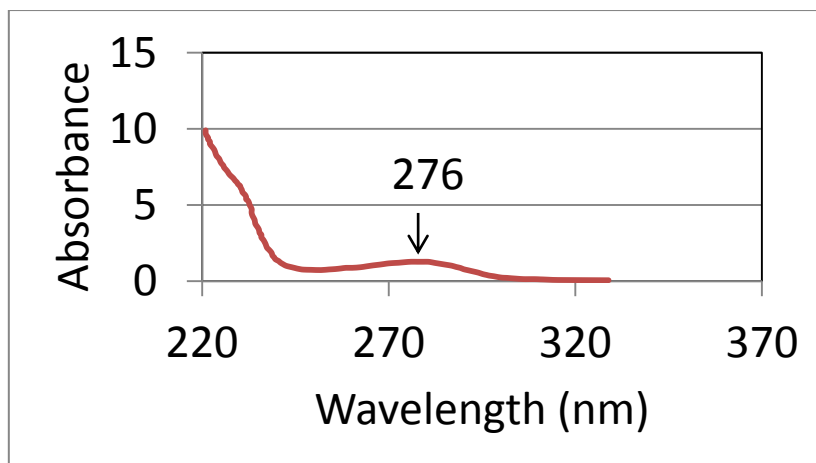


**Figure 33: Protein concentration after dialysis**

The molecular weight of FBP was acquired as 37144 g/mol according to the amino acid sequence from ExPASy. After the iron separation from the holo – protein, the concentration was measured as 1.616 mg/ml and a peak at around 280 nm was obtained (Figure 34). From these results, the molarity of the protein was calculated as 0.044 mM.

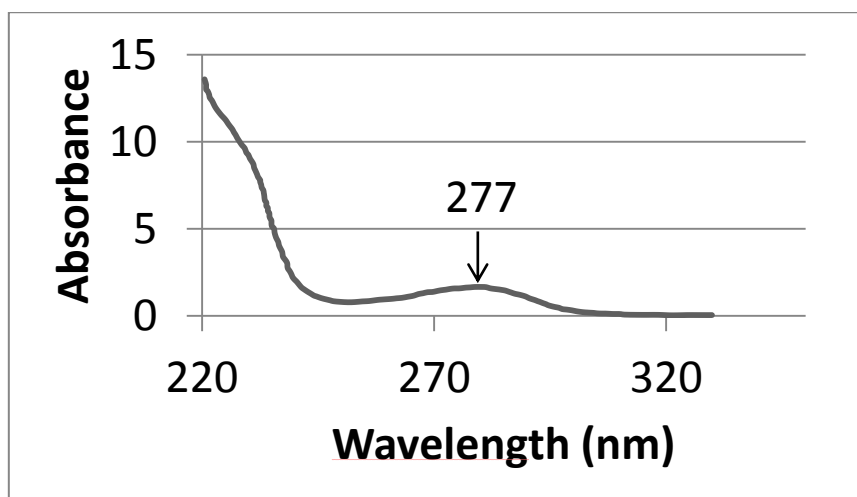


**Figure 34: Protein concentration after the separation of iron**

The protein solution was divided into two tubes and both were concentrated into  $\frac{1}{4}$  by centrifuging in Centricon. Then, the concentration of the protein was measure again and

expected to be four times more concentrated (Figure 35). The concentrations of the protein solution in both tubes were increased up to 4.2 mg/ml. A peak at the 280 nm was obtained.

An additional peak at 230 nm appeared. The molarity was calculated as 0.113 mM.

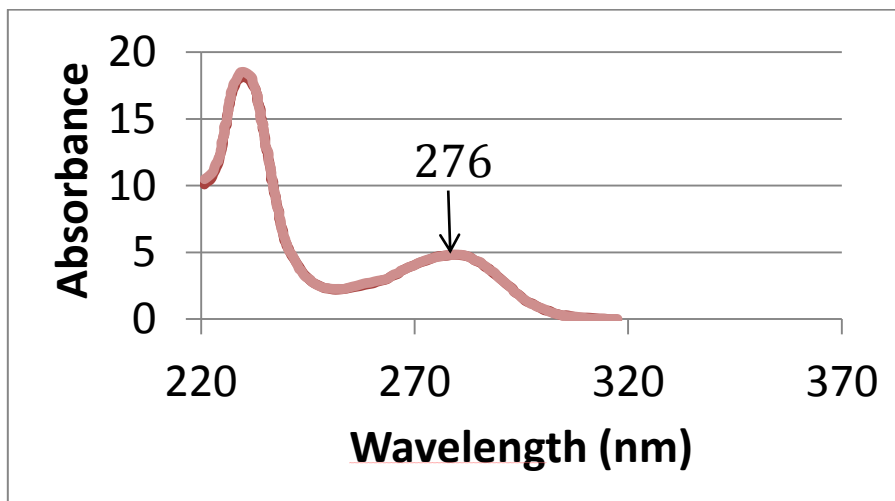


**Figure 35: Increased concentration**

## CHAPTER IV – DISCUSSION

### 4.1. Design and Development of the Microfluidic Device

The pin-fin configuration in the microchannels was expected to increase efficiency of micromixing. With the higher velocities of the flow, the mixing of the two chemicals was provided. However, because of the limitations in high cost of sample volumes, the micromixing channel was needed to be optimized.

Bonding of the PMMA chip was a challenge in this study. Because of the non-homogeneity of the rigid surface material, high flow rates caused the samples to leak in between the layers of PMMA. To avoid leakage, the PMMA plaques were compressed by screws. In such instance, the monitoring regions of the channels were affected by their shadows, and caused limitations in camera recording.

The formidable part of the PDMS design was due to human errors in the fabrication step. Since this process was highly human controlled, it was impossible to do a standardized fabrication of the microchips. The thickness of the chip and the quality of the channels were not standard. This error can be prevented in future designs by practicing more fabrications of such channels.

The cost and time limitations of micromixing chamber optimization became a motivation for running numerical analysis. Simulations provided a quick view and perspective of how to improve the microfluidic design for better mixing efficiency. That the numerical predictions for the current chip correctly identified the observed mixing behavior, we are confident in using the current numerical integration schemes for other designs. From the simulations, we find that the location of the pin-fins in the chamber should be varied. The configuration of the current design was not found as effective as it was originally predicted. Therefore, in the future work different configuration and shape of the pin-fins was targeted to be tested (Figure 27).

On the other hand, generally, protein kinetic studies are done by using stopped flow designs, which give rise to lots of practical considerations. However, our design can be considered as rare because of its continuous flow system. Hence, we avoided all the stopped flow accessories such as complicated optical detection equipment, and problems relating to sudden pressure drop. Also we were able to obtain flow data as a function of distance from the mixing zone by photographing the flow path from side, which allowed us to gather thousands of time data points per photograph as opposed to one or two.

#### **4.2. Expression and Purification of the FBP**

After the expression of the FBP, the cells were lysed to get the protein. In this step, protein solution was observed to have pinkish color, which would suggest that the FBP was expressed in holo form. The flow through sample of the washing step in column purification was transparent as histidine tagged proteins were expected to be attached nickel resin in the column and not to be washed with washing buffer. However, imidazole in elution buffer was accepted as a competitive molecule and detached the proteins from nickel and transferred them into the solution [47]. Therefore, the pinkish color was again observed in the elution. This situation required additional step for removing  $\text{Fe}^{+3}$  ions.

To confirm the proteins' functioning, they were recombined with  $\text{Fe}^{+3}$  ions, via  $\text{FeCl}_3$  titration. For this purpose,  $\text{FeCl}_3$  was prepared in Tris.HCl buffer at pH 8, which was identical to the solution where the proteins were present. Nevertheless,  $\text{FeCl}_3$  happened to be insoluble at the indicated pH. Thus, the  $\text{FeCl}_3$  were prepared in water where the solution became acidic.

## CHAPTER V – CONCLUSION AND FUTURE WORK

### 5.1. Conclusions

In this thesis, a microfluidic based automated system was manufactured. The system was designed and developed to have the following features: (I) compact and cost-efficient; (II) easy to fabricate microfluidic chip; (III) bioavailable and non-toxic materials used in the microfluidic chip, so that they cause no limitation for protein studies; (IV) small sample volumes; (V) minimized design was proper monitoring of fast reactions; (VI) disposable microfluidic chip to eliminate risk of contamination.

We have fabricated microfluidic chips from two different materials. Therefore, we have collected comparable data by using PMMA and PDMS microfluidic chips and fin-pin mixing geometries. For the purposes of monitoring iron binding dynamics of bacterial FBP, we have successfully expressed and purified Haemophilus Influenza FBP by using recombinant DNA technology.

There were also some difficulties we have met. First of all, sealing of the PMMA microfluidic chip was an adversity. Avoiding the fluid to leak in between the layers was a challenge for this study. Similarly, bonding of the PDMS microfluidic chip required testing several materials until an optimal one was determined. Different procedures were followed from the literature to optimize air plasma step in order to provide bonding of the chip surface by a glass slide.

The advantage of our system, besides the listed features, is the simple monitoring. Because the flow is recorded in the microchannels, the captions can be analyzed digitally. Besides a high definition camera, there is no other complicated measurement device required. This is because of the color change from transparent to pink in the iron binding reaction. For systems with no such abrupt color change inherent to the reaction being monitored, attachment of an optical sensor to the design would be required.

Our design is also unique in terms of color inclusion into the analysis. Hence, the idea of using this design can be extended to 1000s of different systems.

## 5.2. Future Work

Characterization of the *Haemophilus Influenzae* FBP will be completed by structural analysis. CD (Circular Dichroism) spectra will be measured to find the conformational features of the protein. As future work, the design described in Figure 27 will be fabricated using PDMS material. After the optimization of mixing chamber, recombinant FBP will be analyzed by combining with  $\text{Fe}^{+3}$  solution and will be monitored. We expect a color gradient from red (the color of iron solution) to be pink (the color of FBP bound to  $\text{Fe}^{+3}$ ) (Figure 35). The reaction will be recorded with a high-resolution camera and analyzed by a program plotting color intensities at certain points. We aim to relate color change to absorbance value to be able to plot the calibration curve, which will later be used to determine iron binding constant of the FBP. The color change is expected to show the same trend line; exponential decay as the color spectrum from red to pink. Therefore, the range will stay between 740 to 630 nm [48].

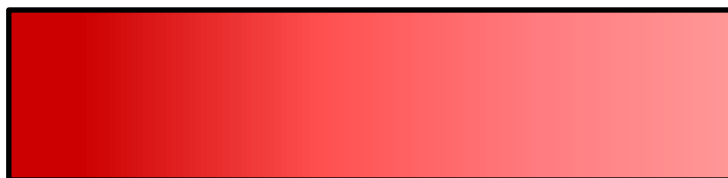


**Figure 36: Expected color gradient**

Future work also contains development of an optical detection compartment, which can detect the absorbance values at certain points along the reaction pathway. For this purpose, the system described in the reference article will be integrated into our design (Figure 36) [17].

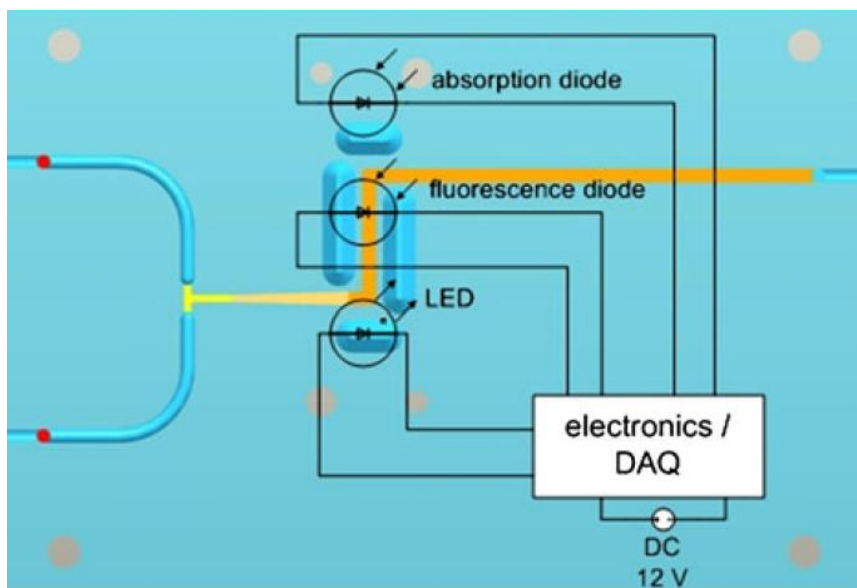


**Figure 37: Optical detection compartment (adapted from ref. [17])**

Kinetic rate data for iron binding protein will be collected from improved microfluidic design in future research. As a result, the unavailability of information in the field will be fulfilled.

## BIBLIOGRAPHY

1. Higgins, C.F., *ABC transporters: from microorganisms to man*. Annual review of cell biology, 1992. **8**(1): p. 67-113.
2. Mietzner, T.A., et al., *Purification and characterization of the major iron-regulated protein expressed by pathogenic Neisseriae*. The Journal of experimental medicine, 1987. **165**(4): p. 1041-1057.
3. Siburt, C.J.P., T.A. Mietzner, and A.L. Crumbliss, *FbpA—A bacterial transferrin with more to offer*. Biochimica et Biophysica Acta (BBA)-General Subjects, 2012. **1820**(3): p. 379-392.
4. Noinaj, N., et al., *Structural basis for iron piracy by pathogenic Neisseria*. Nature, 2012. **483**(7387): p. 53-58.
5. Barber, M.F. and N.C. Elde, *Escape from bacterial iron piracy through rapid evolution of transferrin*. Science, 2014. **346**(6215): p. 1362-1366.
6. Königsberger, L.-C., et al., *Complexation of iron (III) and iron (II) by citrate. Implications for iron speciation in blood plasma*. Journal of inorganic biochemistry, 2000. **78**(3): p. 175-184.
7. Abdizadeh, H., A.R. Atilgan, and C. Atilgan, *Detailed molecular dynamics simulations of human transferrin provide insights into iron release dynamics at serum and endosomal pH*. JBIC Journal of Biological Inorganic Chemistry, 2015. **20**(4): p. 705-718.
8. Wally, J., et al., *The crystal structure of iron-free human serum transferrin provides insight into inter-lobe communication and receptor binding*. Journal of Biological Chemistry, 2006. **281**(34): p. 24934-24944.
9. Steere, A.N., et al., *Kinetics of iron release from transferrin bound to the transferrin receptor at endosomal pH*. Biochimica et Biophysica Acta (BBA)-General Subjects, 2012. **1820**(3): p. 326-333.
10. Aisen, P. and I. Listowsky, *Iron transport and storage proteins*. Annual review of biochemistry, 1980. **49**(1): p. 357-393.
11. Stein, B.S. and H.H. Sussman, *Peptide mapping of the human transferrin receptor in normal and transformed cells*. Journal of Biological Chemistry, 1983. **258**(4): p. 2668-2673.
12. Wooldridge, K.G. and P.H. Williams, *Iron uptake mechanisms of pathogenic bacteria*. FEMS microbiology reviews, 1993. **12**(4): p. 325-348.

13. Taboy, C.H., et al., *Fe<sup>3+</sup> coordination and redox properties of a bacterial transferrin*. Journal of Biological Chemistry, 2001. **276**(4): p. 2719-2724.
14. Bruns, C.M., et al., *Crystallographic and biochemical analyses of the metal-free Haemophilus influenzae Fe<sup>3+</sup>-binding protein*. Biochemistry, 2001. **40**(51): p. 15631-15637.
15. Guven, G., A.R. Atilgan, and C. Atilgan, *Protonation States of Remote Residues Affect Binding–Release Dynamics of the Ligand but Not the Conformation of Apo Ferric Binding Protein*. The Journal of Physical Chemistry B, 2014. **118**(40): p. 11677-11687.
16. Bruns, C.M., et al., *Structure of Haemophilus influenzae Fe<sup>3+</sup>-binding protein reveals convergent evolution within a superfamily*. Nature Structural & Molecular Biology, 1997. **4**(11): p. 919-924.
17. Bleul, R., et al., *Compact, cost-efficient microfluidics-based stopped-flow device*. Analytical and bioanalytical chemistry, 2011. **399**(3): p. 1117-1125.
18. McDonald, J.C. and G.M. Whitesides, *Poly(dimethylsiloxane) as a Material for Fabricating Microfluidic Devices*. Accounts of Chemical Research, 2002. **35**(7): p. 491-499.
19. Whitesides, G.M., *The origins and the future of microfluidics*. Nature, 2006. **442**(7101): p. 368-373.
20. Anderson, J.R., et al., *Fabrication of microfluidic systems in poly (dimethylsiloxane)*. Electrophoresis, 2000. **21**(1): p. 27-40.
21. Ahmed, R., *Optical study on poly (methyl methacrylate)/poly (vinyl acetate) blends*. International Journal of Photoenergy, 2009. **2009**.
22. Kuo, A.C., *Silicone Release Coatings for the Pressure Sensitive Industry—Overview and Trends*. DC Corporation, 2003: p. 1.
23. Richard, A., *Interface and surface effects on the glass-transition temperature in thin polymer films*. Faraday Discussions, 1994. **98**: p. 219-230.
24. Belikov, V., et al., *Material properties database*. Matematicheskoe Modelirovanie, 2014. **26**(8): p. 20-30.
25. Qiu, W., *PDMS Based Waveguides for Microfluidics and EOCB*. 2012, Zhejiang University.
26. Capretto, L., et al., *Micromixing within microfluidic devices*, in *Microfluidics*. 2011, Springer. p. 27-68.

27. Weigl, B.H., R.L. Bardell, and C.R. Cabrera, *Lab-on-a-chip for drug development*. Advanced drug delivery reviews, 2003. **55**(3): p. 349-377.
28. Koşar, A., M.R. Özdemir, and M. Keskinöz, *Pressure drop across micro-pin heat sinks under unstable boiling conditions*. International Journal of Thermal Sciences, 2010. **49**(7): p. 1253-1263.
29. Brackbill, J., D.B. Kothe, and C. Zemach, *A continuum method for modeling surface tension*. Journal of computational physics, 1992. **100**(2): p. 335-354.
30. Eyring, E.M., J.J. Auborn, and P. Warrick Jr, *Spectrophotometric dissociation field effect kinetics of aqueous acetic acid and bromocresol green*. The Journal of Physical Chemistry, 1971. **75**(16): p. 2488-2492.
31. Yu, D., et al., *An efficient recombination system for chromosome engineering in Escherichia coli*. Proceedings of the National Academy of Sciences, 2000. **97**(11): p. 5978-5983.
32. Sauer, B. and N. Henderson, *Site-specific DNA recombination in mammalian cells by the Cre recombinase of bacteriophage P1*. Proceedings of the National Academy of Sciences, 1988. **85**(14): p. 5166-5170.
33. Berg, J.M., J.L. Tymoczko, and L. Stryer, *Restriction Enzymes: Performing Highly Specific DNA-Cleavage Reactions*. 2002.
34. Massey, A. and H. Kreuzer, *Recombinant DNA and Biotechnology: A guide for students*. 2001, Washington, DC: ASM Press. ISBN.
35. Sambrook, J., E.F. Fritsch, and T. Maniatis, *Molecular cloning*. Vol. 2. 1989: Cold spring harbor laboratory press New York.
36. Esposito, D., L.A. Garvey, and C.S. Chakiath, *Gateway cloning for protein expression*, in *High Throughput Protein Expression and Purification*. 2009, Springer. p. 31-54.
37. Kapust, R.B., et al., *Tobacco etch virus protease: mechanism of autolysis and rational design of stable mutants with wild-type catalytic proficiency*. Protein engineering, 2001. **14**(12): p. 993-1000.
38. Hengen, P.N., *Purification of His-Tag fusion proteins from Escherichia coli*. Trends in biochemical sciences, 1995. **20**(7): p. 285-286.
39. Rigaut, G., et al., *A generic protein purification method for protein complex characterization and proteome exploration*. Nature biotechnology, 1999. **17**(10): p. 1030-1032.

40. Stols, L., et al., *A new vector for high-throughput, ligation-independent cloning encoding a tobacco etch virus protease cleavage site*. Protein expression and purification, 2002. **25**(1): p. 8-15.
41. Tang, X., et al., *The optimization of preparations of competent cells for transformation of E. coli*. Nucleic acids research, 1994. **22**(14): p. 2857.
42. Porath, J. and B. Olin, *Immobilized metal affinity adsorption and immobilized metal affinity chromatography of biomaterials. Serum protein affinities for gel-immobilized iron and nickel ions*. Biochemistry, 1983. **22**(7): p. 1621-1630.
43. Laemmli, U.K., *Cleavage of structural proteins during the assembly of the head of bacteriophage T4*. nature, 1970. **227**(5259): p. 680-685.
44. Dyballa, N. and S. Metzger, *Fast and sensitive colloidal coomassie G-250 staining for proteins in polyacrylamide gels*. Journal of visualized experiments: JoVE, 2009(30).
45. Shouldice, S.R., et al., *High resolution structure of an alternate form of the ferric ion binding protein from Haemophilus influenzae*. Journal of Biological Chemistry, 2003. **278**(13): p. 11513-11519.
46. Bradford, M.M., *A rapid and sensitive method for the quantitation of microgram quantities of protein utilizing the principle of protein-dye binding*. Analytical biochemistry, 1976. **72**(1): p. 248-254.
47. Muralidhara, B., et al., *Conformational Flexibility of Mammalian Cytochrome P450 2B4 in Binding Imidazole Inhibitors with Different Ring Chemistry and Side Chains SOLUTION THERMODYNAMICS AND MOLECULAR MODELING*. Journal of Biological Chemistry, 2006. **281**(12): p. 8051-8061.
48. Bruno, T.J. and P.D. Svoronos, *CRC handbook of fundamental spectroscopic correlation charts*. 2005: CRC Press.

## APPENDIX A

### MATERIALS

<b>Name of the Material</b>	<b>Supplier</b>
Plexiglas®	Arkema, France
SU-8 3000	MicroChem, USA
SU-8 Developer	MicroChem, USA
PDMS	Dow Corning, USA
Si-Wafer	Sigma-Aldrich, Germany
Bromocresol Green	Sigma-Aldrich, Germany
Acetic Acid	Merk, Germany
Tyriptide	AppliChem, Germany
NaCl	Sigma-Aldrich, Germany
Yeast Extract	Sigma-Aldrich, Germany
Kanamycin	ThermoFisher Scientific, USA
Agar	AppliChem, Germany
CaCl <sub>2</sub>	Merk, Germany
MgCl <sub>2</sub>	Sigma-Aldrich, Germany
EDTA	Merk, Germany

Tris base	Fluka, Switzerland
HEPES	AppliChem, Germany
NaOH	Sigma-Aldrich
Imidazole	AppliChem, Germany
HCL	Merk, Germany
pET-28a(+)	GenScript, China
Benzonase	Novagen, USA
EDTA-free protease Inhibitor	Roche, Switzerland
BugBuster	Novagen, USA
Ni-NTA Agarose	QUIGEN, Germany
Glycine	Molekula, USA
6X Loading Dye	Fermantas, Germany
Bradford Reagent	Sigma, Germany
Distilled Water	Milipore, France
Ethidium Bromide	Merk, Germany
Liquid Nitrogen	Karbogaz, Turkey
MgCl <sub>2</sub>	Sigma-Aldrich, Germany
Na <sub>2</sub> HPO <sub>4</sub>	Merk, Germany
NdeI Digestion Enzyme	Fermantas, Germany

XhoI Digestion Enzyme	Fermantas, Germany
Miniprep Kit	Quiagen, Germany
Autoclave	Certoclav, Austria
Mass Ruler DNA Ladder	Fermantas, Germany
Gene Ruler	Fermantas, Germany

## APPENDIX B

### EQUIPMENTS

<b>Name of the Equipment</b>	<b>Supplier</b>
Syringe Pump	KD Scientific, USA
Tubing	Festo, Germany
Tygon Tubing	St. Gobain, USA
Fitting	IDEX, Germany
Elbow Connector	EATON, USA
HD Microscope Camera	Vitiny, Poland
Polyolefin Sealing Foil	HJ-BIOANALYTIK, Germany
Micro-Machining Needles	Duratek, Turkey
Harrick Plasma	SciAutomation, Singapore
Vacuum Oven	Shellab, USA
Microliter Pipette	Eppendorf, Germany
Centrifuge	Eppendorf, Germany
Centrifuge	Beckman Coulter, USA
Cuvettes	Cole Palmer, USA
Incubator	Memmert, Germany

Spectrophotometer

Schimadzu, Japan

Vortex

Velp Scientifica, Italy